Supplementary Information

PhD Thesis

02/03/2021

By

Nikita Joseph

Table of Contents

Chapter 2: Continuous Flow Thin Film Microfluidic Mediated Nano Encapsulation of Fish-Oil

1. Optimization of speeds, flow-rates and angles for nano-encapsulation:

Nano-encapsulations were formulated using fish-oil, as a bioactive ingredient, and a mixture of non-ionic surfactant and water. Oil in water nano-encapsulations had a surfactant to oil ratio of 1:1 (w:w) with a total concentration of 2 mg/mL. Briefly, a lipid: oil suspension in water was premixed as an emulsion, then introduced into the borosilicate glass tube (20 mm OD, 17 mm ID) in the VFD through jet-feeds, with the tube rotating at 8000 rpm, at a flow-rate of 0.1 mL/min, with the tilt angle of the tube at 45°, and the device operating at 25°C.

Optimization of flow rates.

1.1 Speeds optimization for nano-encapsulation:

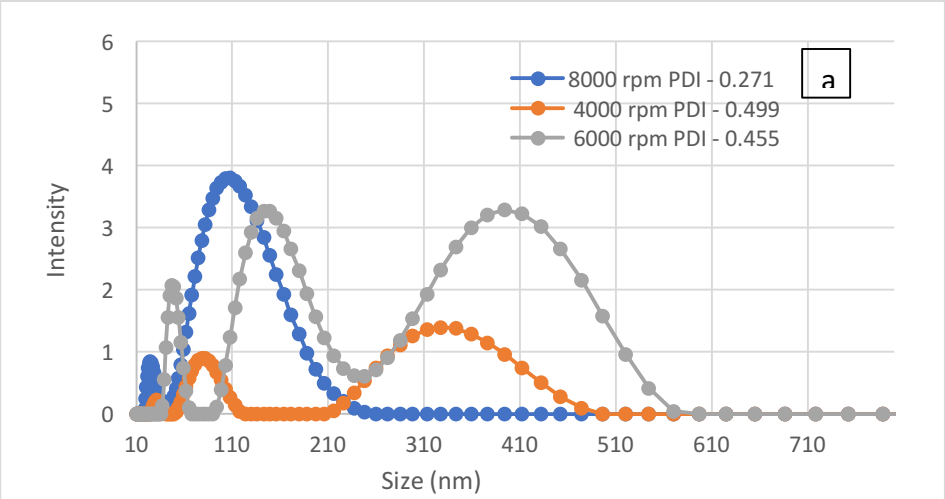

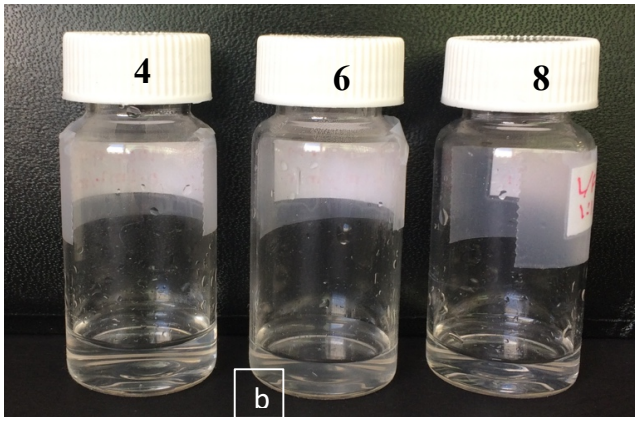

Fig 1.1: (top) (a) DLS data for different speeds i.e. 4000,6000,8000 rpm. (bottom) (b) Physical appearance of solutions at different speeds.

1.2 Flow-rate optimization for nano-encapsulation:

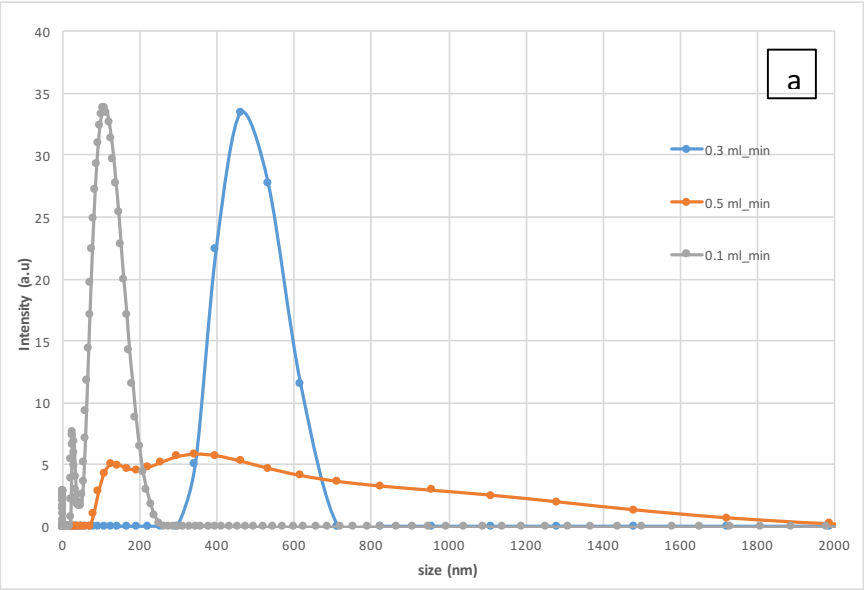

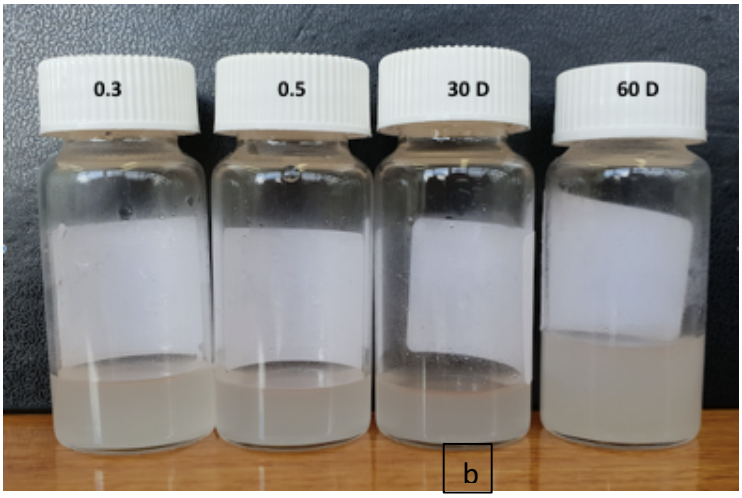

Fig 2: (top) (a) DLS data for different flowrates i.e. 0.1,0.3,0.5 mL/min. (bottom) (b) Physical appearance of solutions at different flowrates and angles.

1.3 Angle optimization for nano-encapsulation:

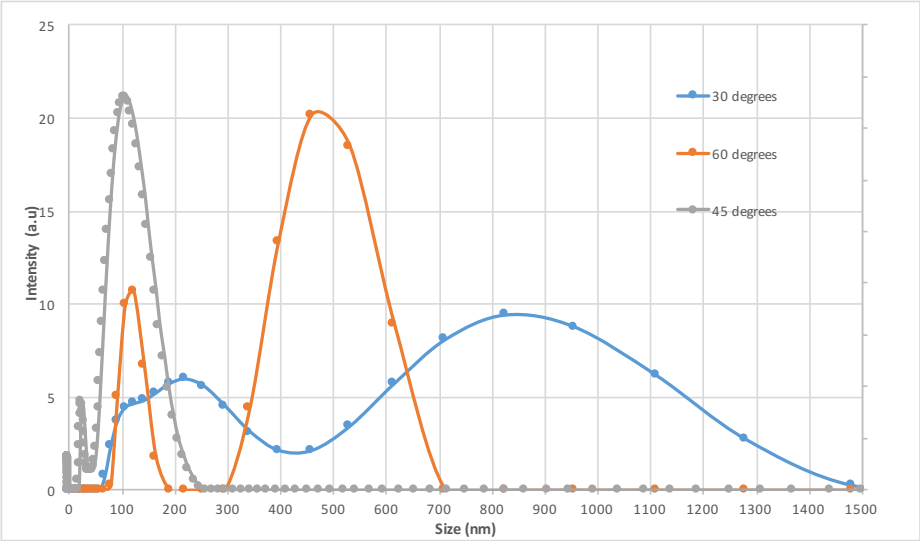

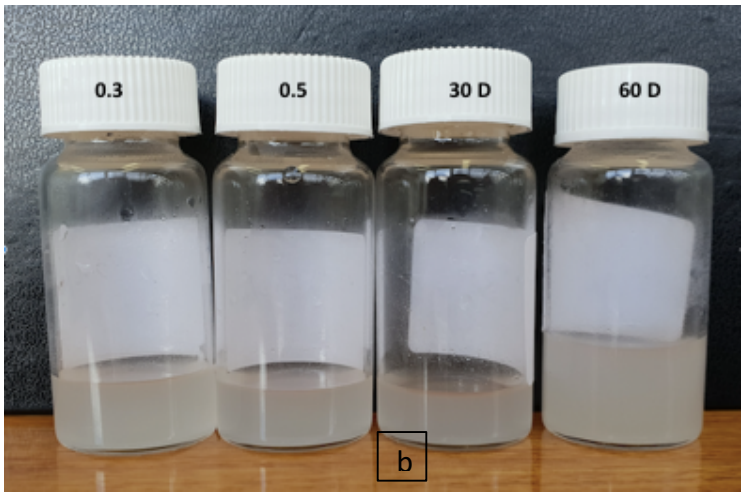

Fig 3: (top) (a) DLS data for different angles 30,45,60 degrees. (bottom) (b) Physical appearance of solutions at different flowrates and angles.

Chapter 3: Vortex Fluidic Mediated Food Processing

1. **Vortex Fluidic Device (VFD)-heating system applied for enzymatic hydrolyzation of protein in milk powder and pasteurization of raw milk.**

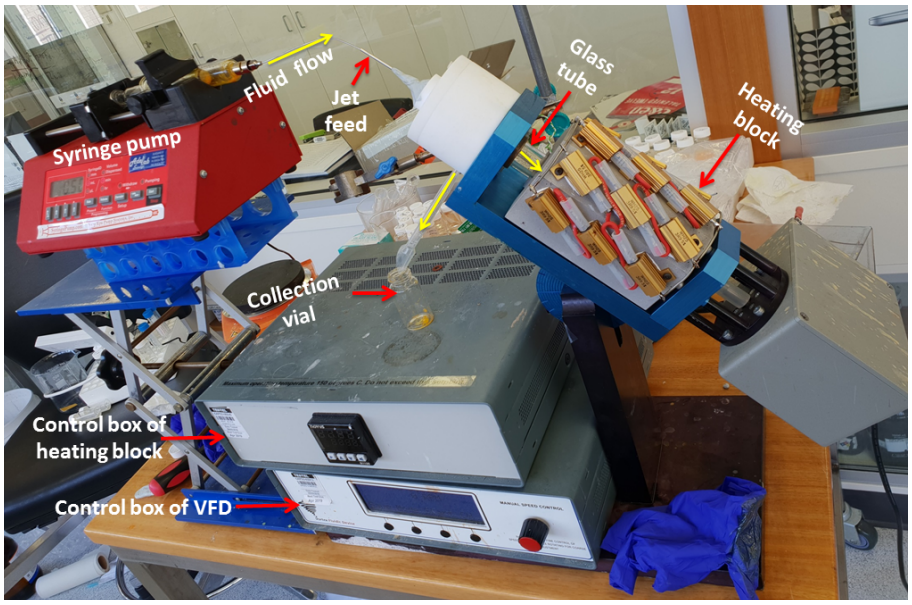

S1 Fig: Photograph of the vortex fluidic device (VFD)-heating system highlighting its salient features

Optimization of the rotational speed, flow-rate and tilt angle for curcumin encapsulation with fish oil and sucrose mono-laurate as an emulsifier

Nano-encapsulations were formulated using curcumin, as a bioactive ingredient, and a mixture of non-ionic surfactant and water. Briefly, 10 mg of curcumin was mixed and dissolved in 60 mg of fish oil. Then the curcumin-fish oil mixture was premixed with 10 mg of sucrose monolaurate and 10 mL of water by using a benchtop vortex mixer, and introduced into the borosilicate glass tube (20 mm OD) in the VFD through jet-feeds, with the tube rotating at 8000 rpm, at a flow-rate of 0.1 mL/min, with the tilt angle of the tube at 45^{o} and the device operating at room temperature. The solution was collected and sonicated for 20 minutes. The data leading up to this optimizing the rotating speed, flow-rate and tilt angle are shown below. The sample produced from optimized conditions was applied to the following UV-visible absorption spectroscopy measurements and fluorescence spectroscopy measurements.

Speed optimization for curcumin encapsulation:

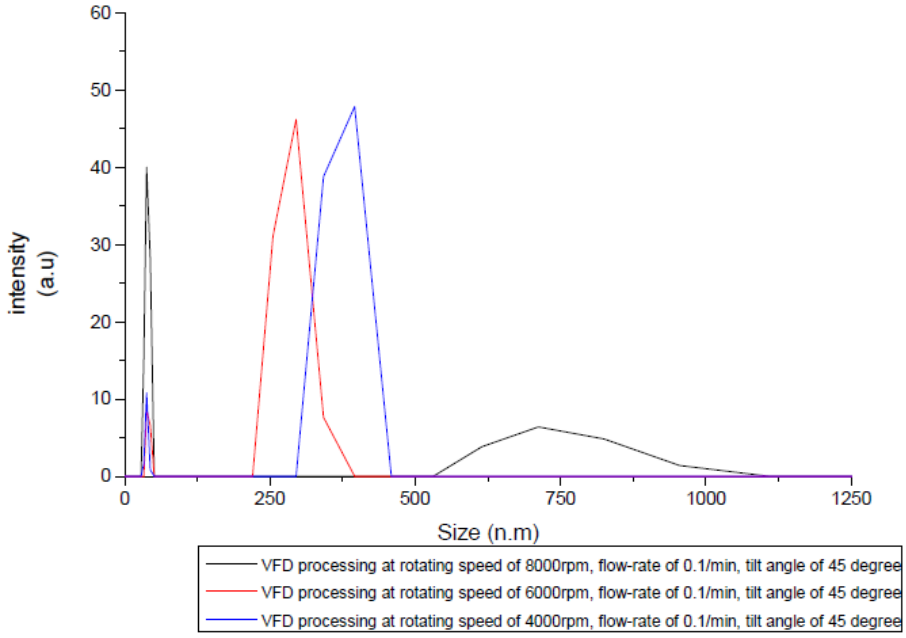

S2 Fig. Dynamic light scattering (DLS) data for preparing encapsulated particles using a vortex fluidic device (VFD) operating at different rotating speeds, for a fixed tilt angle and flow rate.

Flow-rate optimization for Curcumin encapsulation:

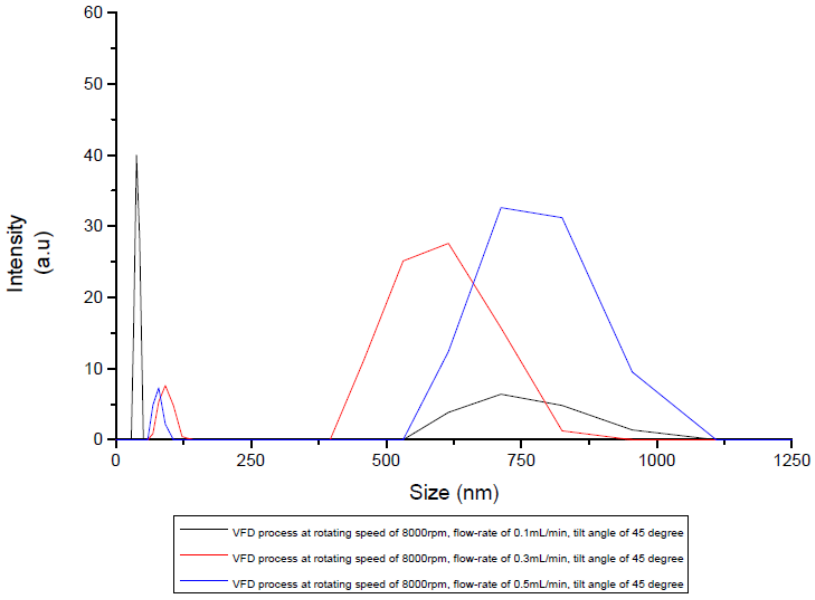

S3 Fig: Dynamic light scattering (DLS) data for preparing encapsulated particles using a vortex fluidic device (VFD) operating at different flow rates, for a fixed tilt angle and rotation speed.

Optimization of the tilt angle for curcumin encapsulation:

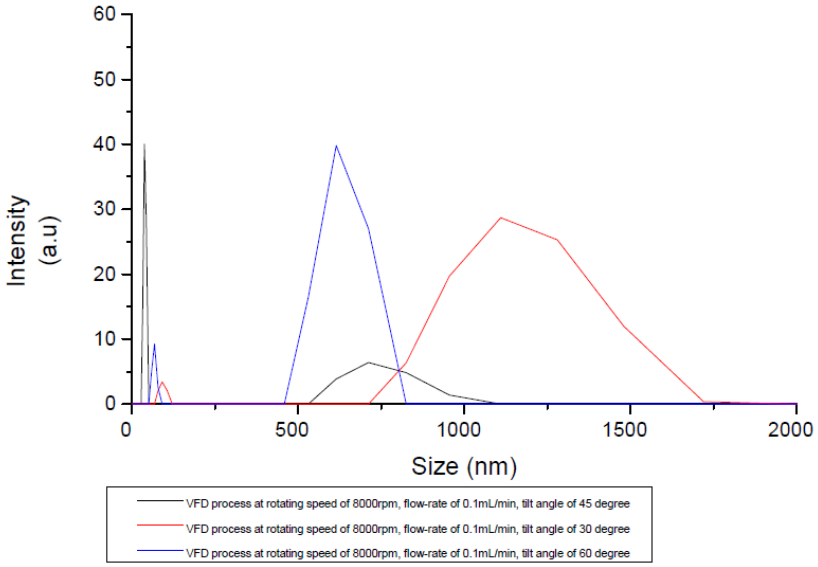

S4 Fig. Dynamic light scattering (DLS) data for preparing encapsulated particles using a vortex fluidic device (VFD) operating at different tilt angles, with a fixed tilt angle and different flow rate.

Chapter 4: Vortex Fluidic Mediated Encapsulation of Functional Fish Oil Featuring *in Situ* Probed Small Angle Neutron Scattering.

1. Rotational speed optimization

Method: Fish-oil emulsions were formulated using a non-ionic surfactant, tween 20 as an emulsiifier and water as the continuous phase. Oil in water emulsions had a surfactant to oil ratio of 1:1 (w:w) with a total concentration of 0.2g/mL. Briefly, a tween 20 and Fish-oil in water was premixed as an emulsion, then introduced into the borosilicate glass tube (20 mm OD, 17 mm ID) in the VFD through jet-feeds, with the tube rotating at different speeds 4000, 5000, 6000, 7000, 8000 and 9000 rpm, at a flow-rate of 0.3 mL/min, with the tilt angle of the tube at 45°, and the device operating at 25°C.

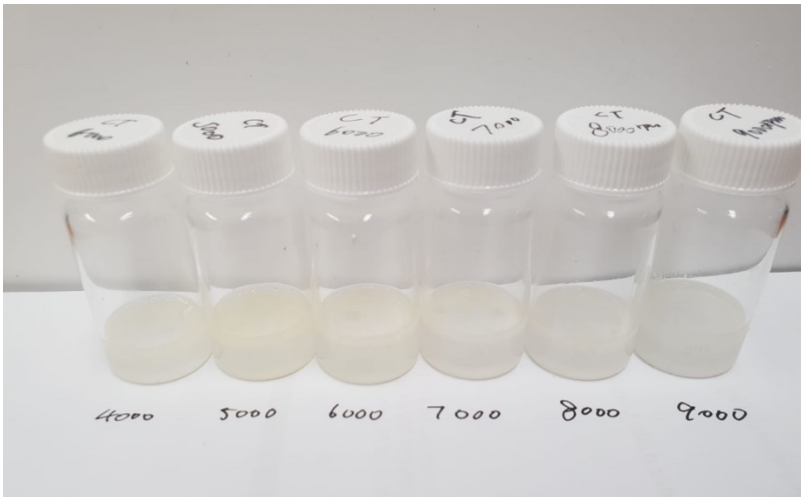

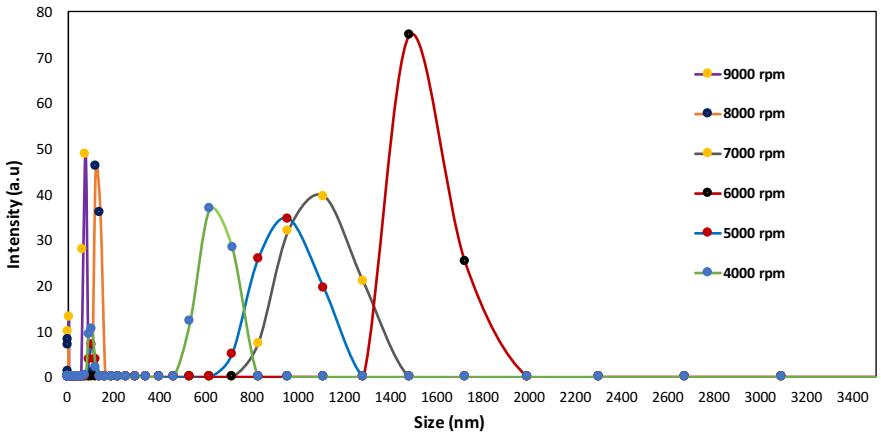

Fig 1: (a) post-VFD vials for fish-oil emulsions processed at speeds 4000 rpm, 5000rpm,6000rpm,7000rpm,8000rpm and 9000 rpm. (b) Dynamic light Scattering (DLS) data for 4000rpm – 9000 rpm. (c) optical microscopy images for speeds 4000 rpm - 9000 rpm.

Optimization of flow rates.

2. Homogenization Surfactant to Oil Ratio (SOR) optimization.

Method: Fish-oil emulsions were formulated using a non-ionic surfactant, tween 20 as an emulsifier and water as the continuous phase. Oil in water emulsions had a surfactant to oil ratio of 1:1, 1:2, 1:3 (w:w) with a total concentration of 0.2g/mL, 0.3g/mL & 0.4g/mL. All the solutions are homogenized at speed of 13,500 rpm for 20 minutes at 25°C.

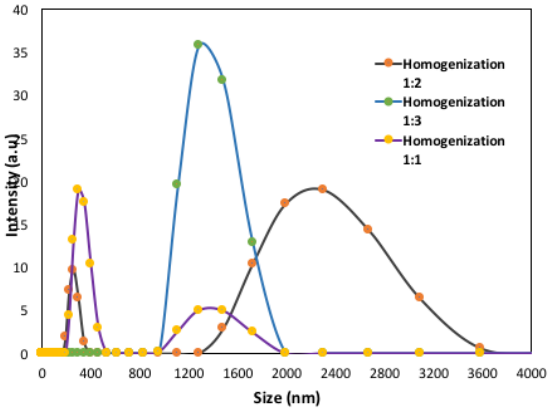

Fig 2: DLS data for all the solutions were homogenized at 13,500 rpm and SOR at 1:1, 1:2, 1:3.

3. VFD Surfactant to Oil Ratio (SOR) optimization

Method: Fish-oil emulsions were formulated using a non-ionic surfactant, tween 20 as an emulsiifier and water as the continuous phase. Oil in water emulsions had a surfactant to oil ratio of 1: 0.5, 1:1, 1:2, 1:3 (w: w) with a total concentration of 0.15g/mL, 0.2g/mL, 0.3g/mL & 0.4g/mL.

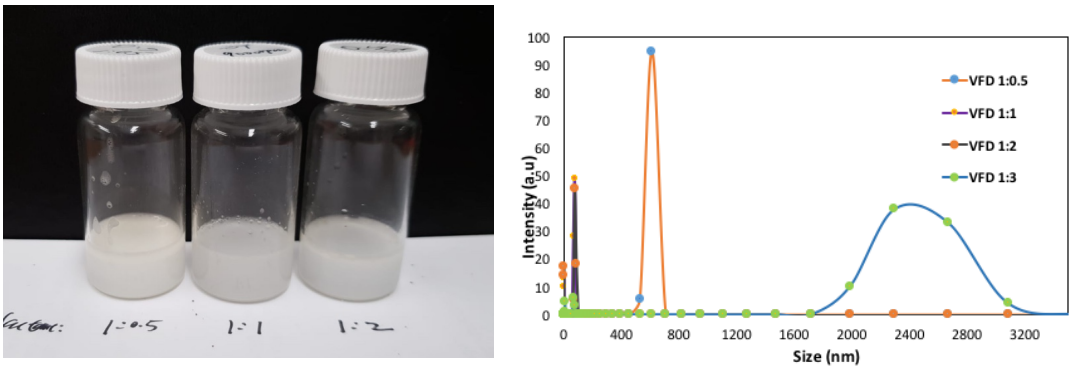

Fig 3: DLS data for all the solutions were processed in VFD at 9000rpm, 0.3 mL/min and SOR at 1:0.5, 1:1, 1:2, 1:3.

4. Flow-rate optimization:

Method: Fish-oil emulsions were formulated using a non-ionic surfactant, tween 20 as an emulsiifier and water as the continuous phase. Oil in water emulsions had a surfactant to oil ratio of 1:1 (w:w) with a total concentration of 0.2g/mL. Briefly, a tween 20 and Fish-oil in water was premixed as an emulsion, then introduced into the borosilicate glass tube (20 mm OD, 17 mm ID) in the VFD through jet-feeds, with the tube rotating at speed 9000 rpm, at a flow-rate of 0.3 mL/min, 0.5 mL/min, 0.7mL/min, 1mL/min with the tilt angle of the tube at 45^{o}, and the device operating at 25°C.

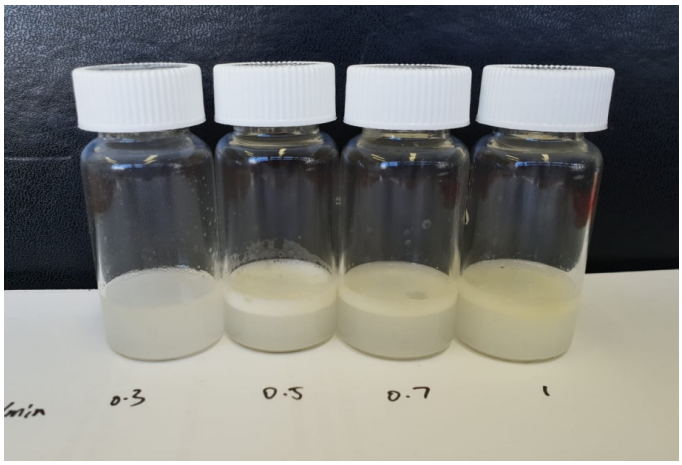

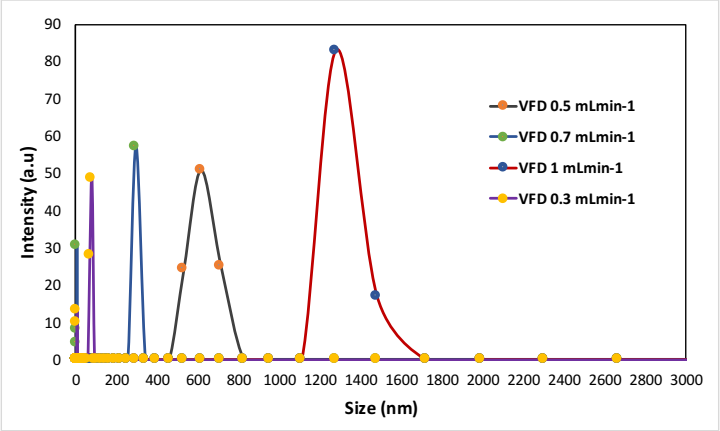

Fig 4: DLS data for all the solutions were processed in VFD at 9000rpm, 0.3 mL/min, 0.5 mL/min, 0.7mL/min, and 1.0mL/min.

5. pH optimization:

Method:

Fish-oil emulsions were formulated using a non-ionic surfactant, tween 20 as an emulsiifier and water as the continuous phase. Oil in water emulsions had a surfactant to oil ratio of 1:1, 1:2 and 1:3 (w:w) with a total concentration of 0.2g/mL, 0.3g/mL and 0.4g/mL. Briefly, a tween 20 and Fish-oil in water was premixed as an emulsion, then introduced into the borosilicate glass tube (20 mm OD, 17 mm ID) in the VFD through jet-feeds, with the tube rotating at speed 9000 rpm, at a flow-rate of 0.3 mL/min and different pH by adjust acid and base at pH 3, pH 5 and pH7.

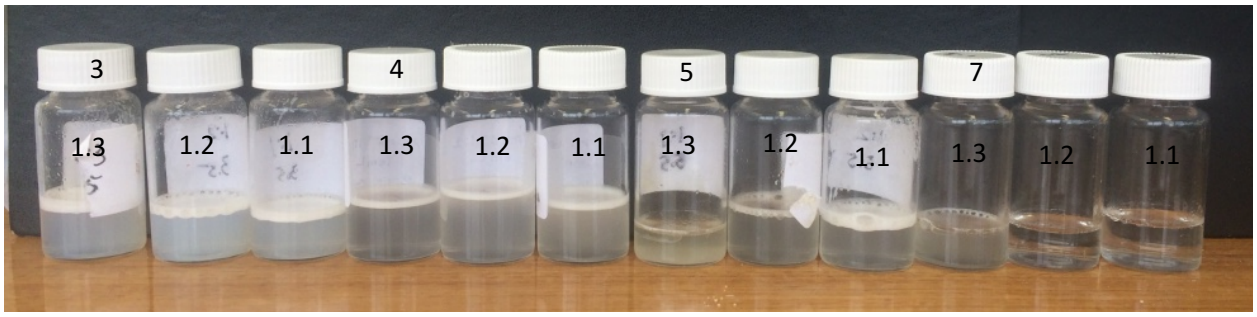

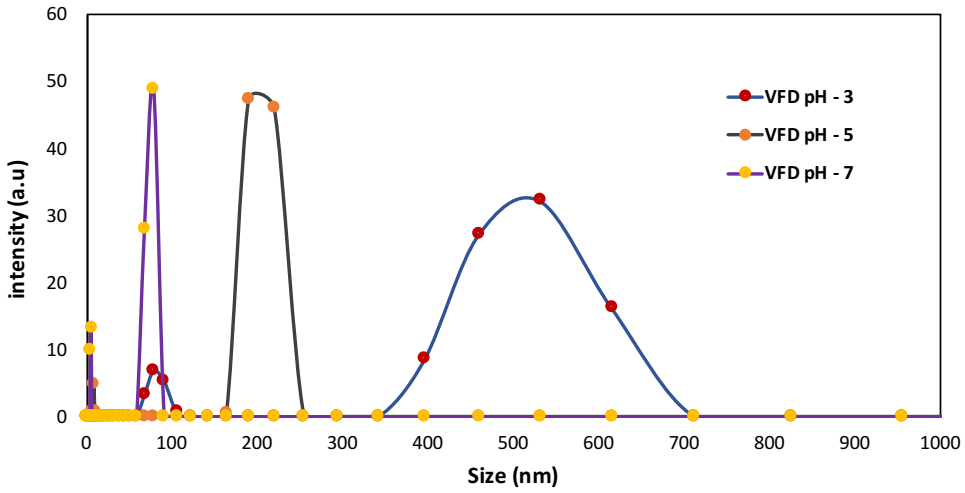

Fig 5: DLS data for all the solutions were processed in VFD at 9000rpm, 0.3 mL/min, SOR 1:1 and different pH at pH3, pH5, pH7.

Emulsion Stability Index

Method

At different rpms, flow-rates, SOR and pH the emulsion stability index is measured.

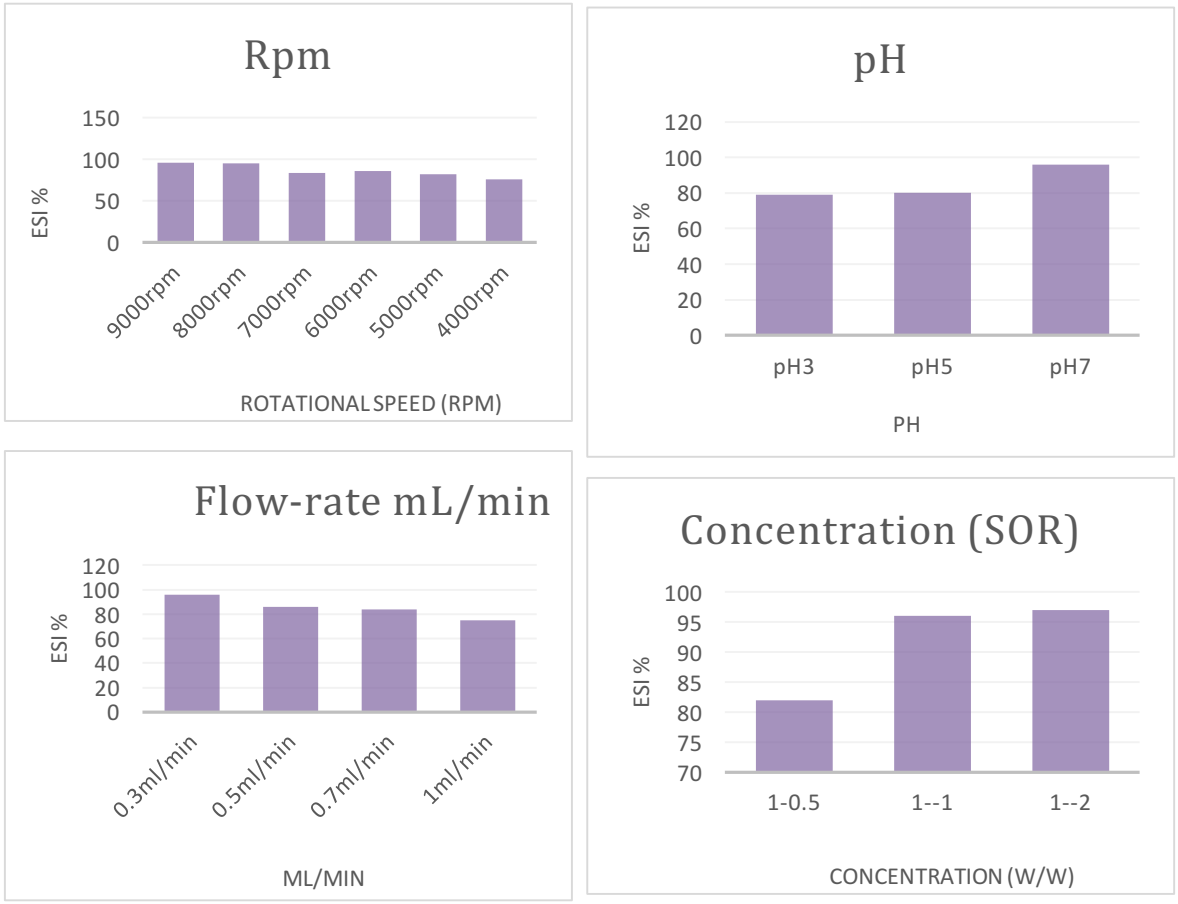

Fig 6: Emulsion Stability Index (ESI) for different rpms, flow-rates, concentration and pH.

Small-angle Neutron Scattering (SANS) Analysis

Method:

SANS was conducted on the BILBY instrument at ANSTO (Lucas Heights, NSW, Australia). The VFD was setup in BILBY's sample staging area so scans could be made of the sample in the VFD while it is being sheared (real-time VFD). After the sample was sheared, it was scanned again with static-SANS to determine if the VFD had any lasting effects on the sample structure. The data was reduced to account for the instrument geometry, detector resolution, and background scattering from solvent, the quartz VFD tube, and the environment, and was then set to absolute scale. The data was then analyzed with the NIST macros for Igor Pro. The scattering length densities (SLDs) for the materials in the samples were calculated using NIST's online neutron activation and scattering calculator (https://www.ncnr.nist.gov/resources/activation/) using the molecular formulae and densities shown in Table S1. The best fit for each data set is shown below. Non-resolution-smeared models had to be used to fit the data due to the large q-resolution interfering with the quality of the fits. The sqrt(χ^2/N) values were not reported for the fits, as they were misleadingly large due to an issue with the wide-angle transmission correction applied during the reduction step in Mantid, which caused the intensity error estimates to be greatly overestimated. The rationale for the choice in models and the significance of the fitting results were discussed in the article.

Table S1: SLDs for each material.

Material:	Molecular Formula:	Density (g/mL):	SLD:
Tween 20	$C_{58}H_{114}O_{26}$	1.1	5.594e-07
Fish Oil	$C_{60}H_{92}O_6$	0.9	5.5165e-07
D_2O	D_2O	1.1	6.4e-6

Tween 20 in D_2O, 0 rpm VFD (Unsmeared Gauss Sphere with Screened Coloumb Interaction)

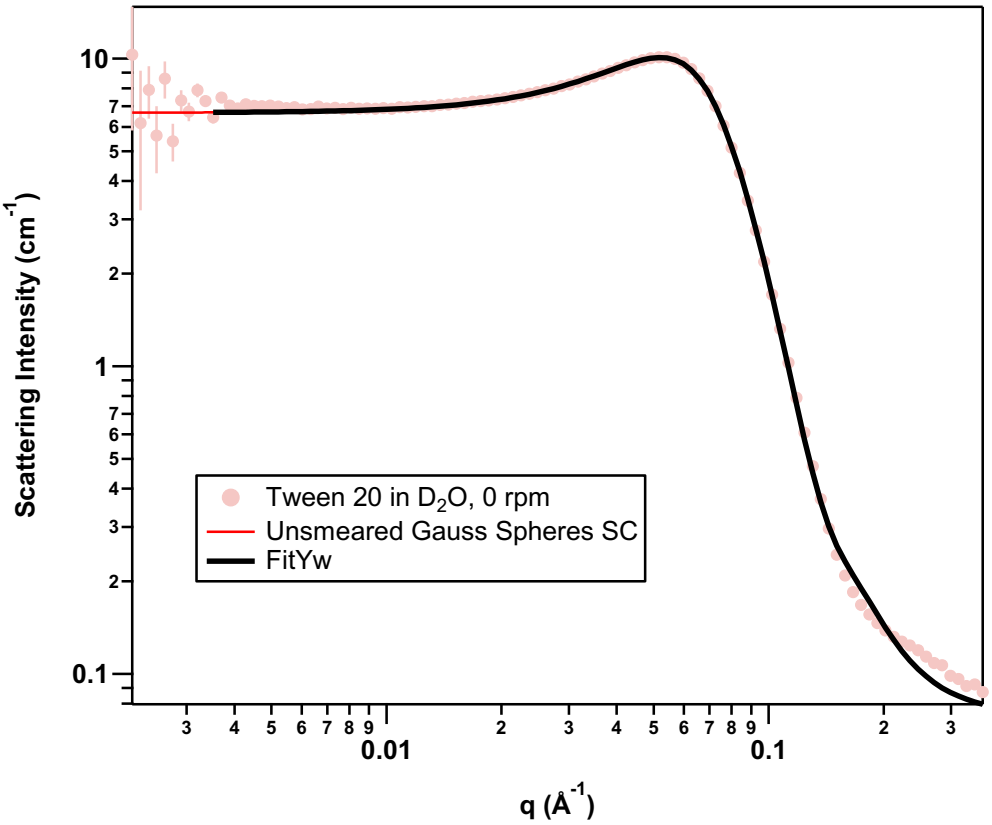

Volume Fraction (scale)	0.0491582	±	1.90914e-05
mean radius (Å)	25.9163	±	0.0157088
polydisp (sig/avg)	0.266229	±	0.000651247
SLD sphere ($Å^{-2}$)	5.594e-07	±	0
SLD solvent ($Å^{-2}$)	6.4e-06	±	0
charge	26.0198	±	0.166143
movalent salt(M)	0.0522068	±	0.000395825
Temperature (K)	293	±	0
dielectric const	78	±	0
bkg ($cm^{-1}·sr^{-1}$)	0.0733463	±	0.000199529
Fitted Range	0.00352	< Q <	0.36309

Tween 20 in D_2O, 4000 rpm VFD (Unsmeared Gauss Sphere with Screened Coloumb Interaction)

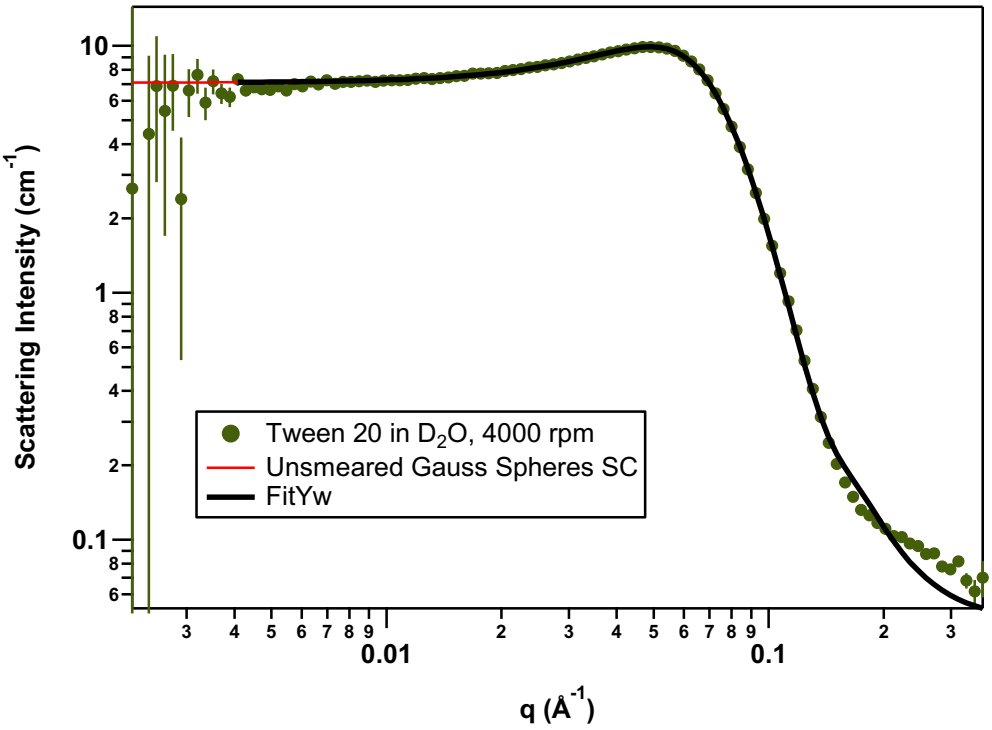

Volume Fraction (scale)	0.0461051	±	5.31792e-05
mean radius (Å)	26.0389	±	0.0494433
polydisp (sig/avg)	0.270393	±	0.00197293
SLD sphere ($Å^{-2}$)	5.594e-07	±	0
SLD solvent ($Å^{-2}$)	6.4e-06	±	0
charge	20.8297	±	0.283647
movalent salt(M)	0.0432632	±	0.000763135
Temperature (K)	293	±	0
dielectric const	78	±	0
bkg ($cm^{-1}·sr^{-1}$)	0.0468341	±	0.000648175
Fitted Range	0.00408	< Q <	0.36309

Tween 20 in D_2O, post-4000 rpm (Unsmeared Gauss Sphere with Screened Coloumb Interaction)

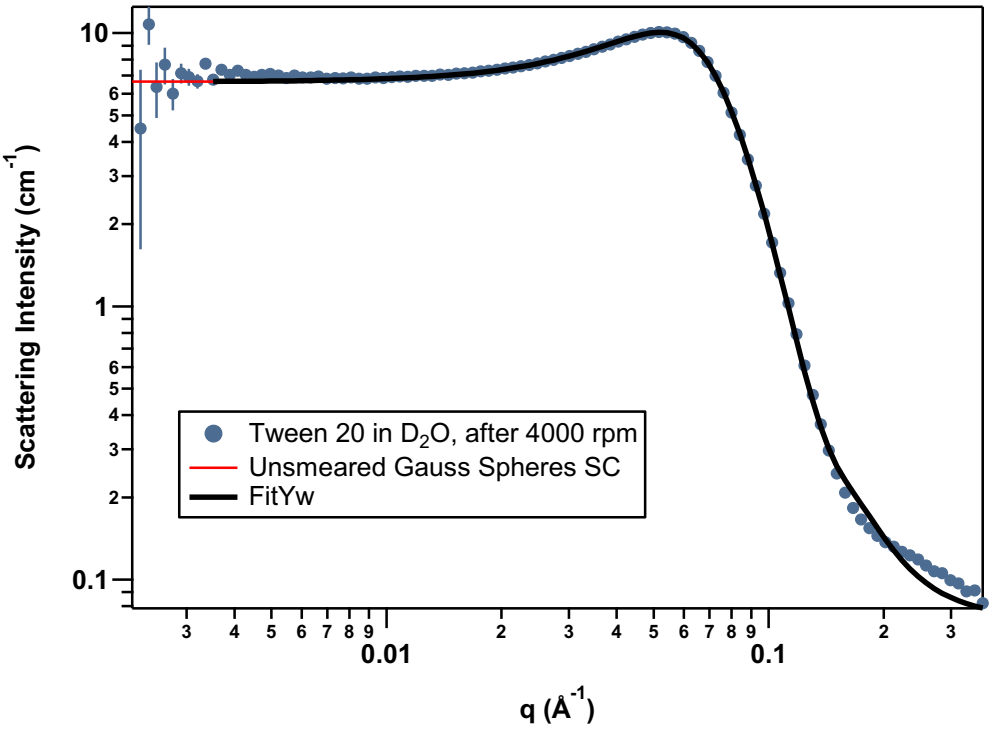

Volume Fraction (scale)	0.0491837	±	1.97642e-05
mean radius (Å)	25.8611	±	0.0162959
polydisp (sig/avg)	0.26787	±	0.00067638
SLD sphere ($Å^{-2}$)	5.594e-07	±	0
SLD solvent ($Å^{-2}$)	6.4e-06	±	0
charge	25.0828	±	0.158155
movalent salt(M)	0.0499541	±	0.000381678
Temperature (K)	293	±	0
dielectric const	78	±	0
bkg ($cm^{-1}·sr^{-1}$)	0.0725075	±	0.000204008
Fitted Range	0.00352	< Q <	0.36309

Tween 20 in D_2O, 7000 rpm VFD (Unsmeared Gauss Sphere with Screened Coloumb Interaction)

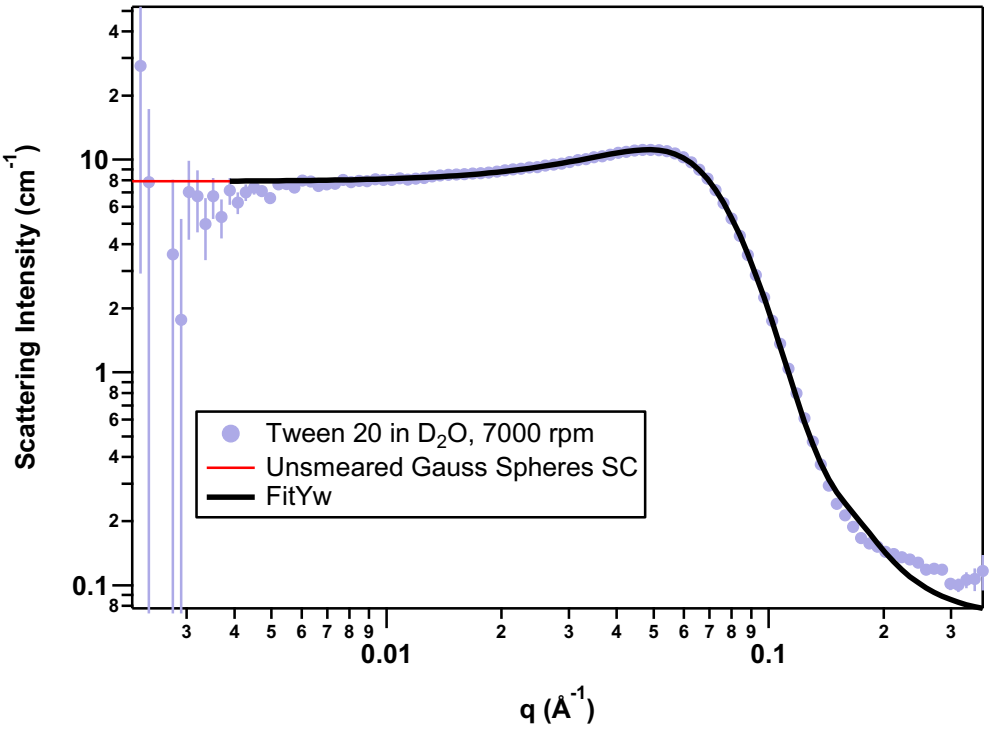

Volume Fraction (scale)	0.0523772	±	0.00010129
mean radius (Å)	25.9333	±	0.0798426
polydisp (sig/avg)	0.286116	±	0.00323363
SLD sphere ($Å^{-2}$)	5.594e-07	±	0
SLD solvent ($Å^{-2}$)	6.4e-06	±	0
charge	14.8518	±	0.177749
movalent salt(M)	0.0290873	±	0.000569441
Temperature (K)	293	±	0
dielectric const	78	±	0
bkg ($cm^{-1}·sr^{-1}$)	0.0712808	±	0.00116415
Fitted Range	0.00389	< Q <	0.36309

Tween 20 in D_2O, post-7000 rpm (Unsmeared Gauss Sphere with Screened Coloumb Interaction)

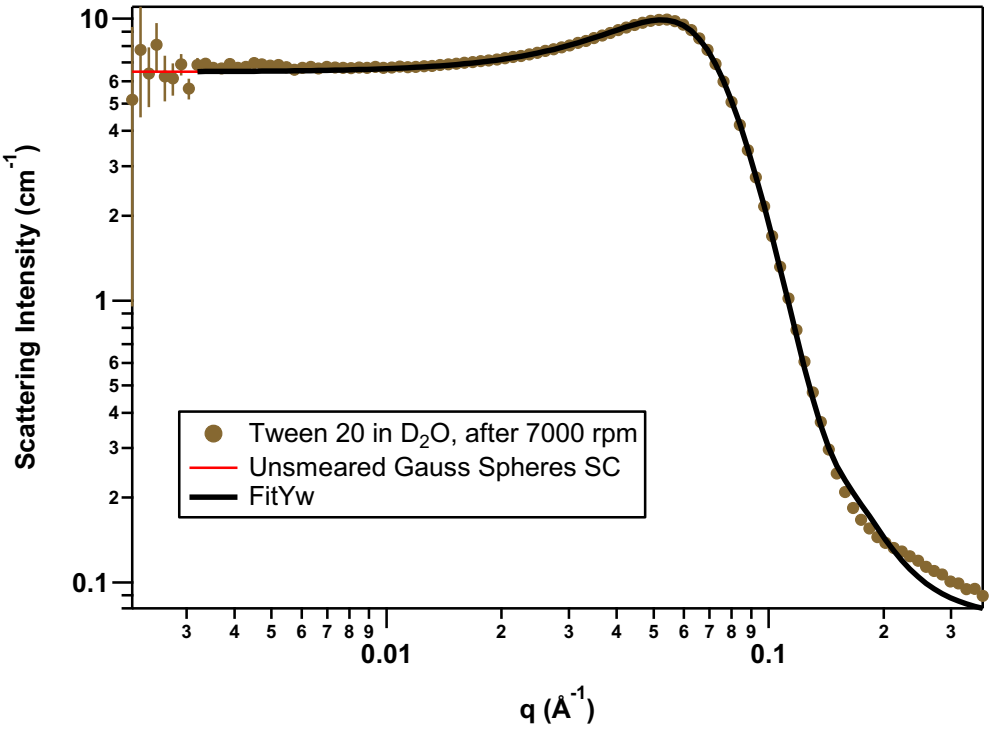

Volume Fraction (scale)	0.0484201	±	1.98097e-05
mean radius (Å)	25.8657	±	0.0165874
polydisp (sig/avg)	0.264747	±	0.000688993
SLD sphere ($Å^{-2}$)	5.594e-07	±	0
SLD solvent ($Å^{-2}$)	6.4e-06	±	0
charge	28.115	±	0.208806
movalent salt(M)	0.0556216	±	0.00047066
Temperature (K)	293	±	0
dielectric const	78	±	0
bkg ($cm^{-1}·sr^{-1}$)	0.074726	±	0.000206961
Fitted Range	0.0032	< Q <	0.36309

Tween 20 in D_2O, 9000 rpm VFD (Unsmeared Gauss Sphere with Screened Coloumb Interaction)

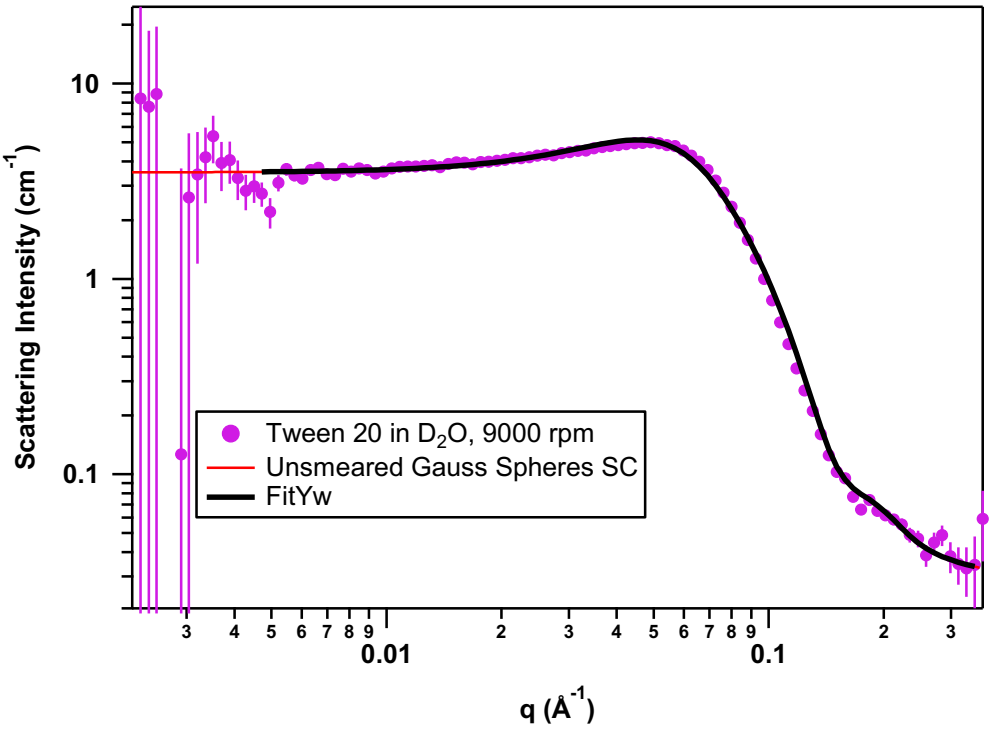

Volume Fraction (scale)	0.0225735	±	1.84241e-05
mean radius (Å)	25.753	±	0.00714267
polydisp (sig/avg)	0.215761	±	0.000254697
SLD sphere ($Å^{-2}$)	5.594e-07	±	0
SLD solvent ($Å^{-2}$)	6.4e-06	±	0
charge	31.1659	±	0.126163
movalent salt(M)	0.0416523	±	0.000170985
Temperature (K)	293	±	0
dielectric const	78	±	0
bkg ($cm^{-1}·sr^{-1}$)	0.03	±	0
Fitted Range	0.00472	< Q <	0.3458

Tween 20 in D_2O, post-9000 rpm (Unsmeared Gauss Sphere with Screened Coloumb Interaction)

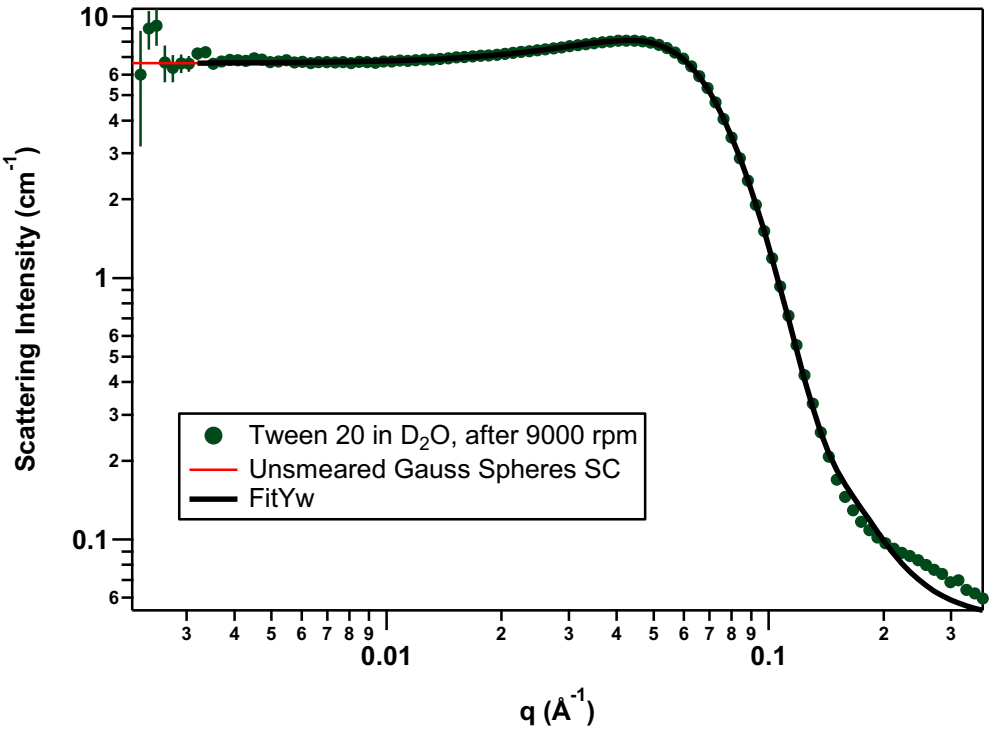

Volume Fraction (scale)	0.0346468	±	1.47213e-05
mean radius (Å)	25.6145	±	0.0213655
polydisp (sig/avg)	0.280512	±	0.000813097
SLD sphere ($Å^{-2}$)	5.594e-07	±	0
SLD solvent ($Å^{-2}$)	6.4e-06	±	0
charge	19.9039	±	0.142842
movalent salt(M)	0.0434194	±	0.000385316
Temperature (K)	293	±	0
dielectric const	78	±	0
bkg ($cm^{-1}·sr^{-1}$)	0.0491574	±	0.000185349
Fitted Range	0.0032	< Q <	0.36309

Tween 20 and Fish Oil in D_2O, 0 rpm (Unsmeared Power Law + Gauss Sphere with Screened Coloumb Interaction)

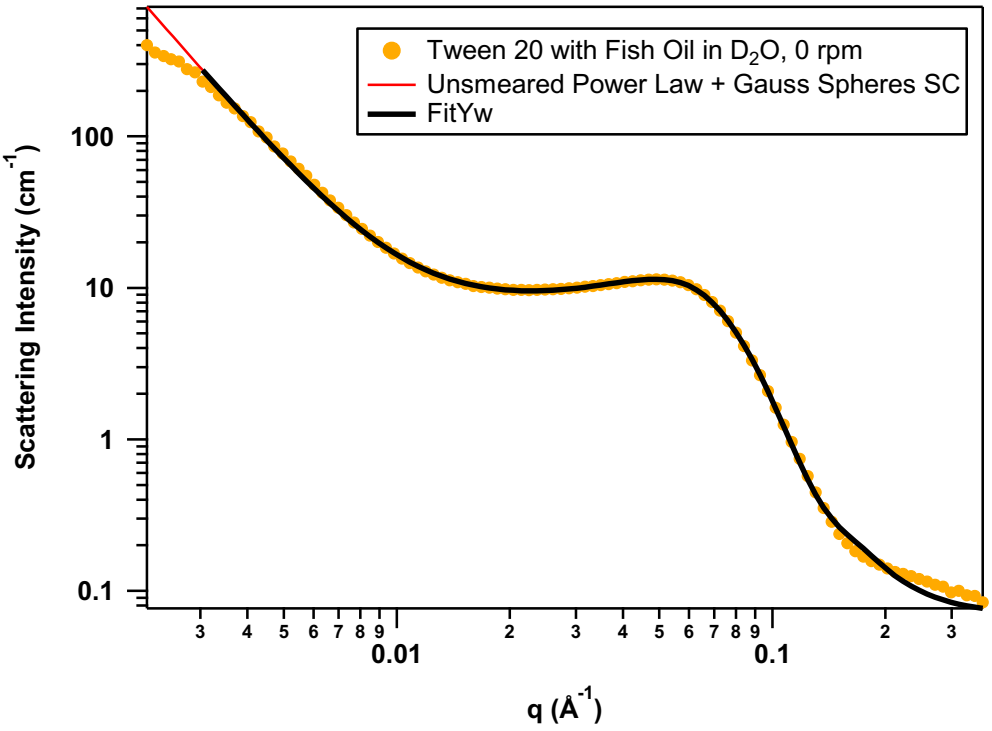

Coefficient, A	1.67248e-05	±	2.26231e-07
(-)Power	2.86139	±	0.00265228
Volume Fraction (scale)	0.0500488	±	1.94136e-05
mean radius (Å)	26.5523	±	0.0162621
polydisp (sig/avg)	0.276035	±	0.0006534
SLD sphere ($Å^{-2}$)	5.594e-07	±	0
SLD solvent ($Å^{-2}$)	6.4e-06	±	0
charge	17.4371	±	0.0777869
movalent salt(M)	0.0300579	±	0.000217549
Temperature (K)	293	±	0
dielectric const	78	±	0
bkg ($cm^{-1}\cdot sr^{-1}$)	0.0701039	±	0.00020354
Fitted Range	0.00304	< Q <	0.36309

Tween 20 and Fish Oil in D_2O, 4000 rpm VFD (Unsmeared Power Law + Gauss Sphere)

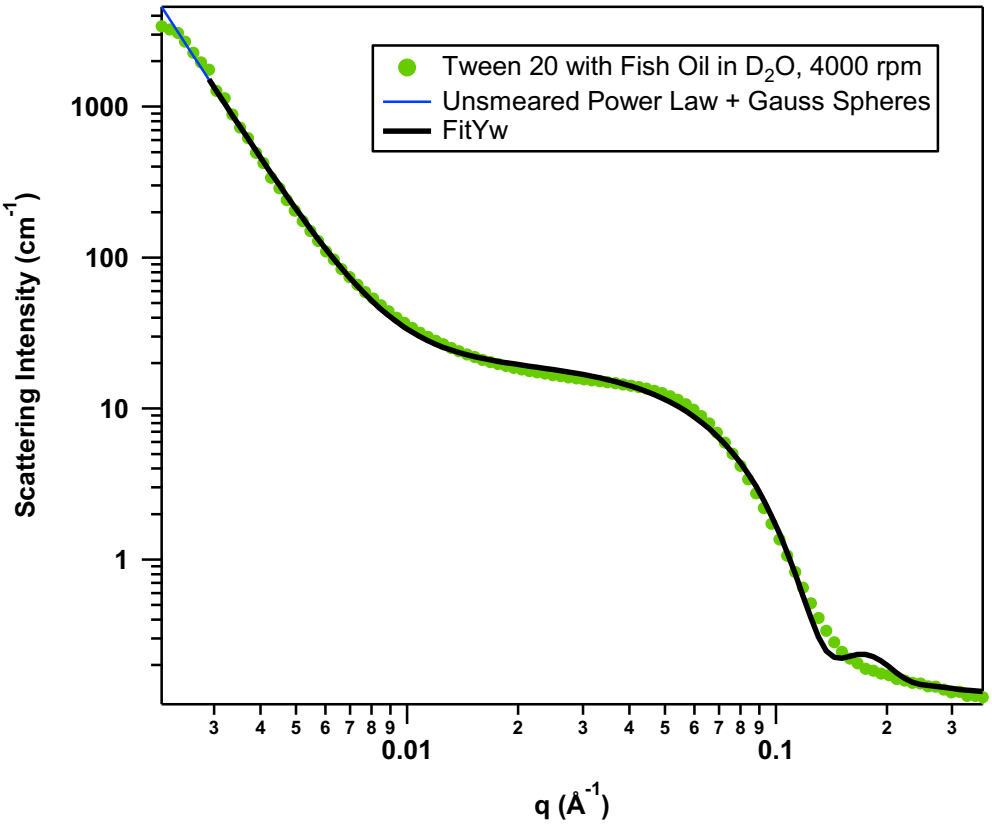

Coefficient, A	3.6337e-07	±	6.20295e-09
(-)Power	3.78876	±	0.00328761
Volume Fraction (scale)	0.0415249	±	1.9324e-05
mean radius (Å)	30.3142	±	0.0186125
polydisp (sig/avg)	0.134407	±	0.000634907
SLD sphere ($Å^{-2}$)	5.594e-07	±	0
SLD solvent ($Å^{-2}$)	6.4e-06	±	0
bkg ($cm^{-1}\cdot sr^{-1}$)	0.128526	±	0.000566774
Fitted Range	0.0029	< Q <	0.36309

Tween 20 and Fish Oil in D_2O, post-4000 rpm (Unsmeared Power Law + Gauss Sphere with Screened Coloumb Interaction)

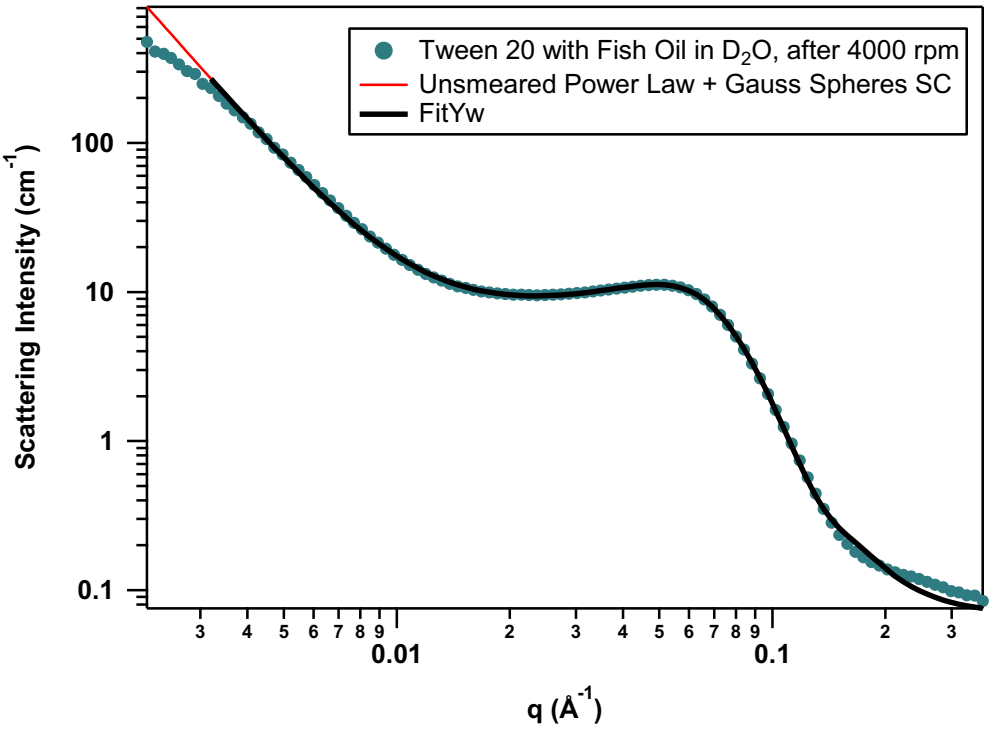

Coefficient, A	1.75396e-05	±	2.02722e-07
(-)Power	2.87542	±	0.00227496
Volume Fraction (scale)	0.049501	±	1.80949e-05
mean radius (Å)	26.5235	±	0.0152951
polydisp (sig/avg)	0.273322	±	0.000615288
SLD sphere ($Å^{-2}$)	5.594e-07	±	0
SLD solvent ($Å^{-2}$)	6.4e-06	±	0
charge	18.5937	±	0.0840211
movalent salt(M)	0.0323293	±	0.000226673
Temperature (K)	293	±	0
dielectric const	78	±	0
bkg ($cm^{-1}\cdot sr^{-1}$)	0.0689952	±	0.000193849
Fitted Range	0.0032	< Q <	0.36309

Tween 20 and Fish Oil in D_2O, 7000 rpm VFD (Unsmeared Power Law + Gauss Sphere)

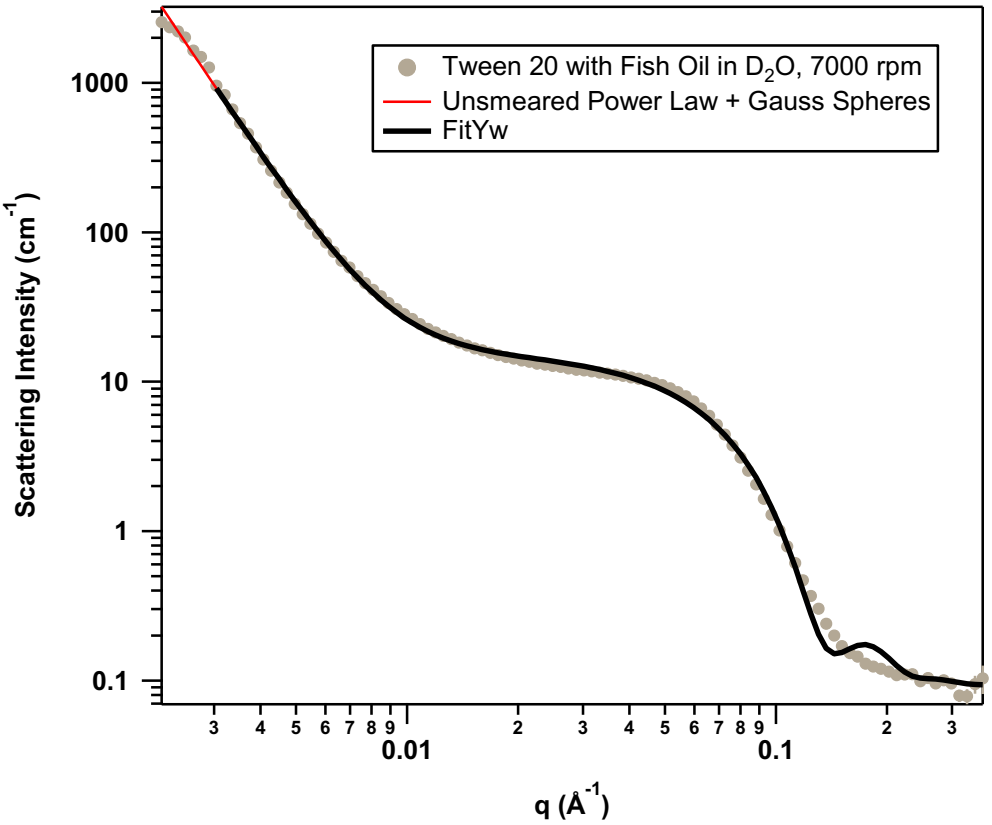

Coefficient, A	4.26267e-07	±	1.17156e-08
(-)Power	3.70541	±	0.00531275
Volume Fraction (scale)	0.0310748	±	2.78394e-05
mean radius (Å)	30.8248	±	0.0349945
polydisp (sig/avg)	0.118497	±	0.00125168
SLD sphere ($Å^{-2}$)	5.594e-07	±	0
SLD solvent ($Å^{-2}$)	6.4e-06	±	0
bkg ($cm^{-1}·sr^{-1}$)	0.0899289	±	0.000937647
Fitted Range	0.00304	< Q <	0.36309

Tween 20 and Fish Oil in D_2O, post-7000 rpm (Unsmeared Power Law + Gauss Sphere with Screened Coloumb Interaction)

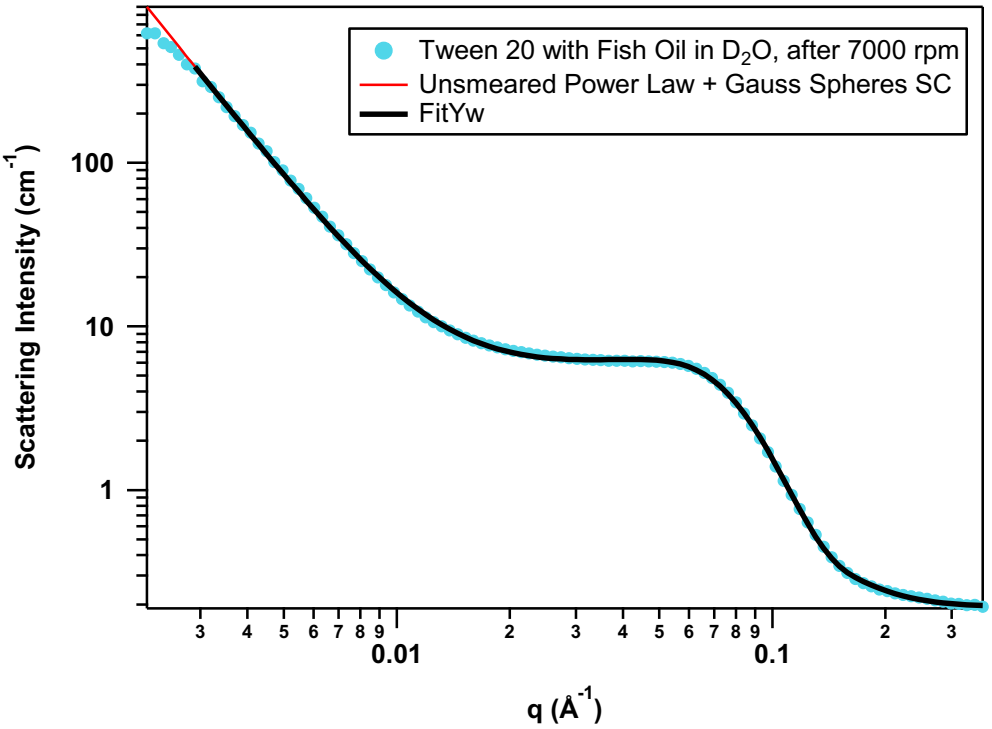

Coefficient, A	1.87394e-05	±	1.75553e-07
(-)Power	2.88023	±	0.00187852
Volume Fraction (scale)	0.0320992	±	8.33743e-06
mean radius (Å)	22.8838	±	0.00210388
polydisp (sig/avg)	0.313201	±	7.49565e-05
SLD sphere ($Å^{-2}$)	5.54e-07	±	0
SLD solvent ($Å^{-2}$)	6.4e-06	±	0
charge	24.8013	±	0.0394279
movalent salt(M)	0.0661625	±	8.48542e-05
Temperature (K)	298	±	0
dielectric const	78	±	0
bkg ($cm^{-1}\cdot sr^{-1}$)	0.191801	±	0.000162145
Fitted Range	0.0029	< Q <	0.36309

Tween 20 and Fish Oil in D_2O, 9000 rpm VFD (Unsmeared Power Law + Gauss Sphere)

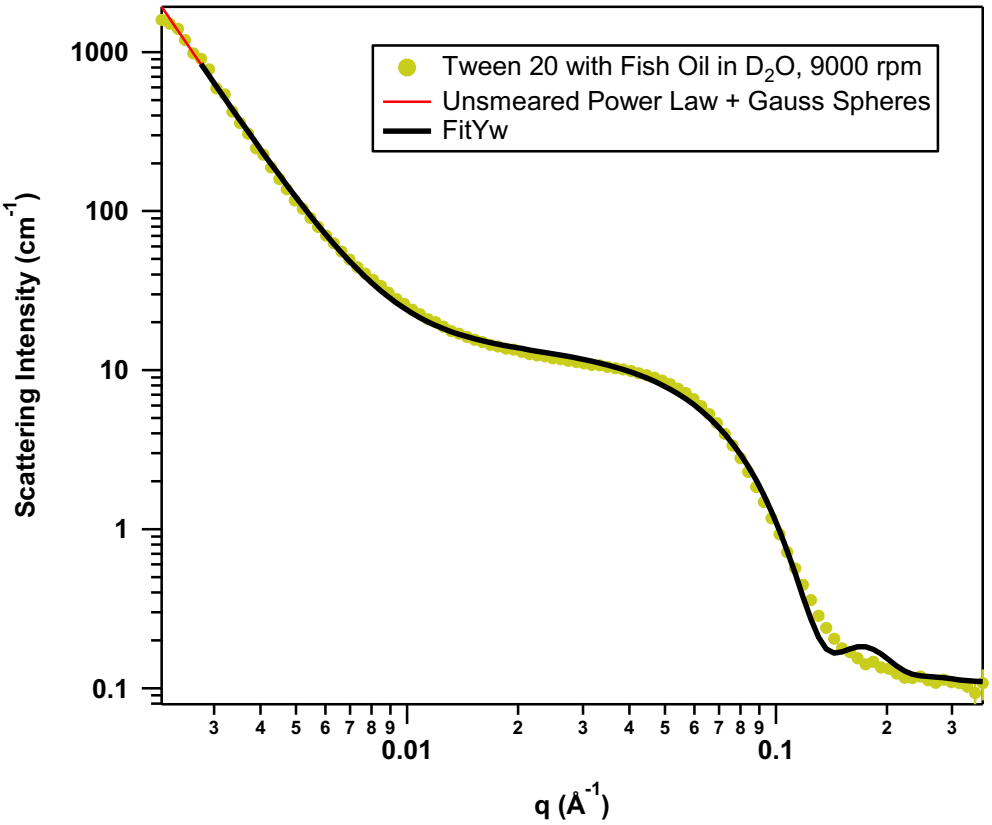

Coefficient, A	1.44004e-06	±	4.40265e-08
(-)Power	3.4226	±	0.00592043
Volume Fraction (scale)	0.0278299	±	2.92026e-05
mean radius (Å)	30.9363	±	0.0419327
polydisp (sig/avg)	0.12419	±	0.00144607
SLD sphere ($Å^{-2}$)	5.594e-07	±	0
SLD solvent ($Å^{-2}$)	6.4e-06	±	0
bkg ($cm^{-1}\cdot sr^{-1}$)	0.106728	±	0.000999342
Fitted Range	0.00276	< Q <	0.36309

Tween 20 and Fish Oil in D_2O, post-9000 rpm (Unsmeared Power Law + Gauss Sphere with Screened Coloumb Interaction)

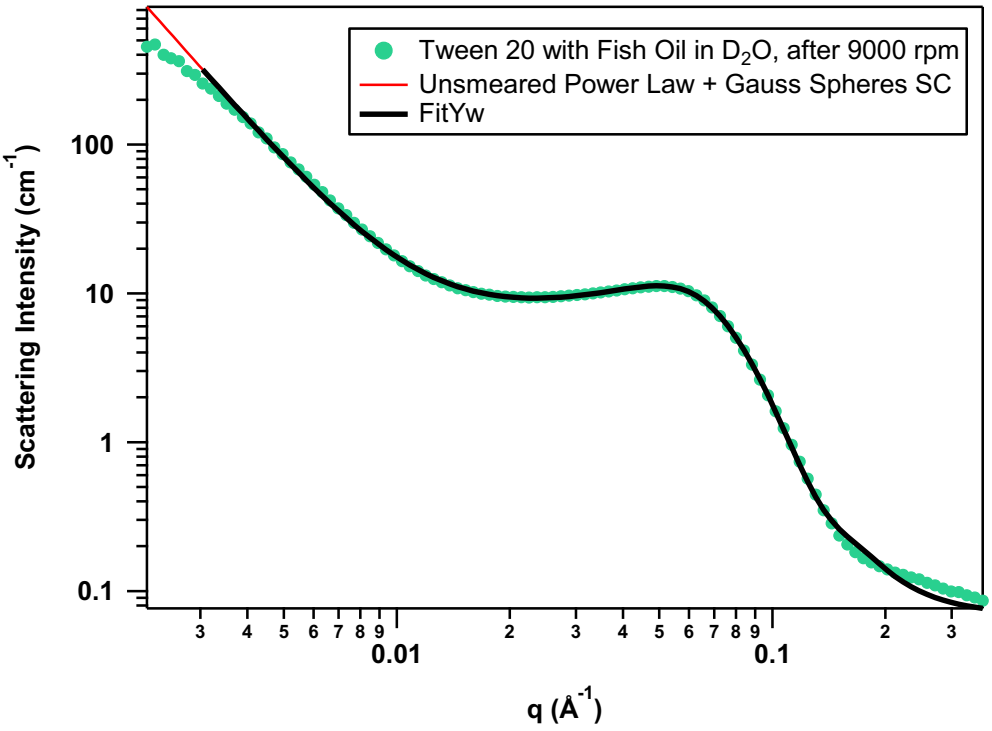

Coefficient, A	1.8384e-05	±	2.16209e-07
(-)Power	2.87254	±	0.00231284
Volume Fraction (scale)	0.0494103	±	1.88022e-05
mean radius (Å)	26.5957	±	0.0158112
polydisp (sig/avg)	0.269822	±	0.000636704
SLD sphere ($Å^{-2}$)	5.594e-07	±	0
SLD solvent ($Å^{-2}$)	6.4e-06	±	0
charge	18.7068	±	0.0894523
movalent salt(M)	0.0311911	±	0.00023252
Temperature (K)	293	±	0
dielectric const	78	±	0
bkg ($cm^{-1}·sr^{-1}$)	0.069991	±	0.000202247
Fitted Range	0.00304	< Q <	0.36309

Chapter 5: Vortex Fluidics Mediated Non-Covalent Physical Entanglement of Tannic Acid and Gelatin for Entrapment of Nutrients.

1. Optimization of the rotational speed, flow-rate and tilt angle for preparing cross-linked gel

Gels were formulated using gelatin and tannic acid. At the optimized condition, gelatin and tannic acid were mixed with a pH of 6. Briefly, the mixed solution was introduced into the borosilicate glass tube (20 mm OD, 17 mm ID) in the VFD through a jet-feed, with the tube rotating at 7000 rpm, at a flow-rate of 0.3 mL/min, with the tilt angle of the tube at 45°, and the device operating at room temperature. The data for optimizing the rotating speed, flow-rate and tilt angle are shown below:

Speed optimization:

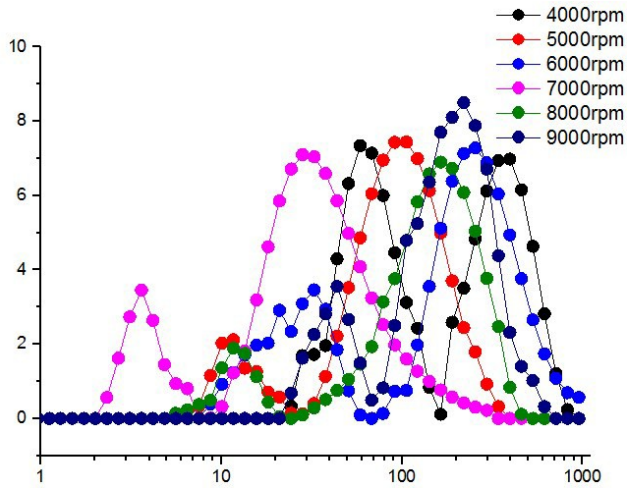

Figure S1. Dynamic light scattering (DLS) data for cross-linked gels prepared using a vortex fluidic device (VFD) operating at different rotating speeds, for a fixed tilt angle (45°) and flow rate (0.3 mL/min).

Flow-rate optimization:

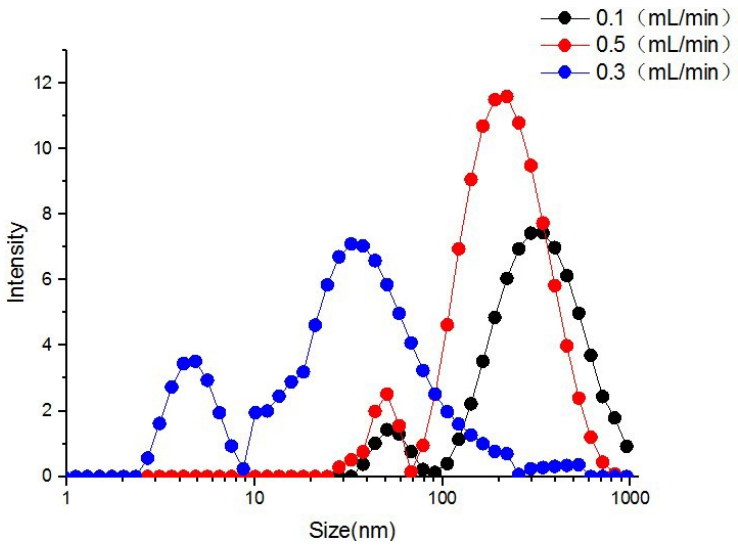

Figure S2. Dynamic light scattering (DLS) data for cross-linked gels prepared using a vortex fluidic device (VFD) operating at different flow rate, with a fixed rotational speed (7000 rpm) and tilt angle(45).

Angle optimization:

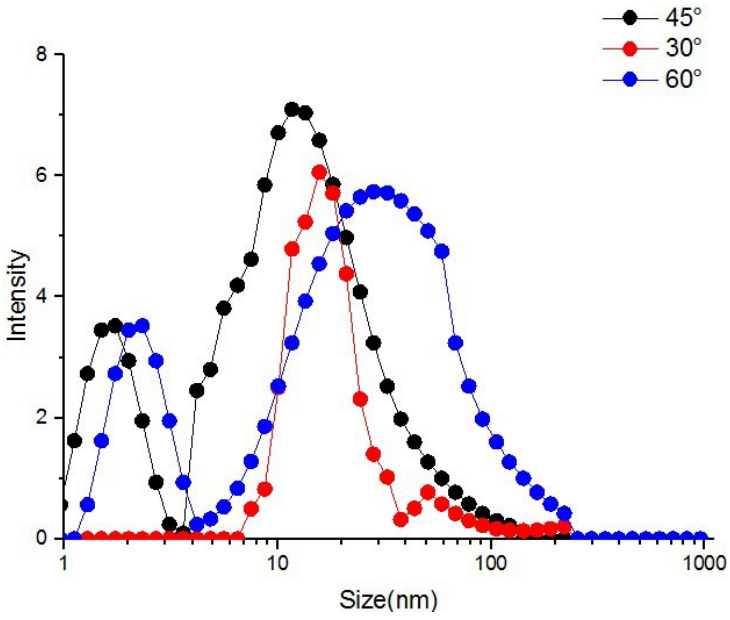

Figure S3. Dynamic light scattering (DLS) data for cross-linked gels using a vortex fluidic device (VFD) operating at different tilt angles, with a fixed rotational speed (7000 rpm) and fixed flow rates (0.3 mL/mi

Chapter 6: Vortex fluidic regulated equilibria involving liposomes down to solvated phospholipids

Nikita Joseph[1,5], Marzieh Mirzamani[2,5], Tarfah Abudiyah[1], Ahmed Alanataki[1], Matt Jellicoe[1], David P Harvey[1], Emily Crawley[1], Andrew Whitten[4], Elliot Gilbert[4], Michael Michael[3], Harshita Kumari[2*], Colin L Raston[1*]

[1] Flinders Institute for Nanoscale Science and Technology (INST), College of Science and Technology, Flinders University, Bedford park, SA 5042 Australia

[2] James L. Winkle College of Pharmacy, University of Cincinnati, Cincinnati, OH 45267-0004, USA

[3] Flinders Centre for Innovation in Cancer (FCIC), Flinders Medical Centre (FMC), Bedford Park, SA 5042 Australia

[4] Australian Nuclear Science and Technology Organization (ANSTO), Lucas heights, NSW 2234 Australia.

[5] Co-first Authors.

[*]Corresponding Authors

Prof. Colin L Raston

Email: colin.raston@flinders.edu.au

Prof. Harshita Kumari

Email: kumariha@ucmail.uc.edu

Contents

1. General materials and methods.

All the chemicals were used as received unless otherwise stated. 1-palmitoyl-2-oleoyl-sn-glycero-3-phosphocholine (POPC) was purchased from Sapphire Biosciences NSW 2016. Trichlorododecaylsilane ≥ 95.0% (GC) for the treatment of hydrophobic surface of the glass tube was purchased from Sigma Aldrich NSW 2016. All the solutions were prepared at room temperature unless otherwise stated using Milli Q water. 1,2-dipalmitoyl-sn-glycero-3-phosphoethanolamine-N-(7-nitro-2-1,3-benzoxadiazol-4-yl) (ammonium salt) 16:0 NBD-PE and 1,2-dipalmitoyl-sn-glycero-3-phosphoethanolamine-N-(lissamine rhodamine B sulfonyl) (ammonium salt) 16:0 (Liss Rh-PE) was purchased from Avanti Polar Lipids USA. All the samples for Australian Nuclear Science and Technology Organization (ANSTO) experiments were prepared in 100% D2O.

All the liposomes samples were analyzed by Dynamic Light Scattering (DLS) using particle sizer DLS (Nano ZS90, Malvern instruments, Worcester, UK). scanning electron microscopy (SEM) performed using a FEI Quanta 450, atomic force microscopy (AFM) using the Nanoscope 8.10 in tapping mode, Transmission Electron Microscopy (TEM) Samples were prepared by drop-casting the material onto standard carbon coated copper grids prior to characterization. Real-time SANS experiments were done at the Australian Nuclear Science and Technology Organization (ANSTO), using the Quokka instrument.

2. Effect on the size of liposomes processed in hydrophobic tube.

Phospholipid suspension at a concentration of 25 μg/mL in confined mode, 1mL of the sample volume and at an angle 45° was processed in a hydrophilic surface VFD tube at 9000 rpm and characterized with Dynamic Light Scattering (DLS) (Red) and compared the same conditions in a hydrophobic surface tube (Green) and characterized using Dynamic Light Scattering (DLS). After treating the VFD surface the size distribution changes from micron range (red) towards 100 nm (green) in size. The hydrophobic nature of the tube controls the self-assembly more towards nm scale region.

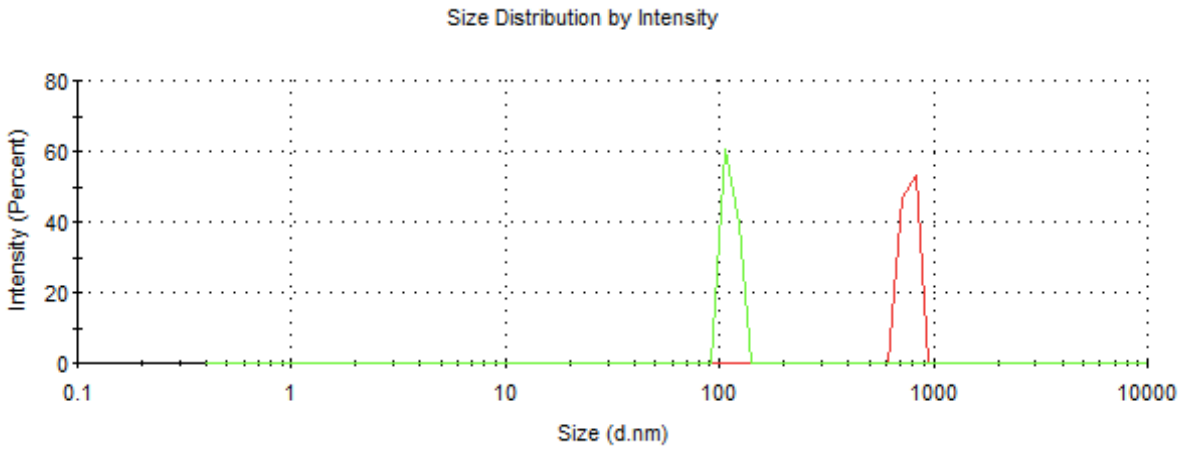

Fig S1: Phospholipid suspension at 25 μg/mL in confined mode, 1mL of the sample volume and at an angle 45°. All the samples were characterized at room temperature 25°C. Hydrophilic tube sample (red) and hydrophobic tube sample is (green). The glass tubes OD was 20mm.

3. Rotational speed optimization in hydrophobic tube.

Phospholipid suspension at a concentration of 25 µg/mL in continuous flow at a flow rate of 0.1 mL/min, tilt angle 45° and in hydrophobic coated tube was processed at speeds 4000 rpm, 5000 rpm, 6000 rpm, 7000 rpm, 8000 rpm, 9000 rpm. All the samples were characterized by DLS. All the rotational speeds were optimized. 9000 rpm was optimized with size range of 100 – 200 nm and PDI of 0.2 – 0.3.

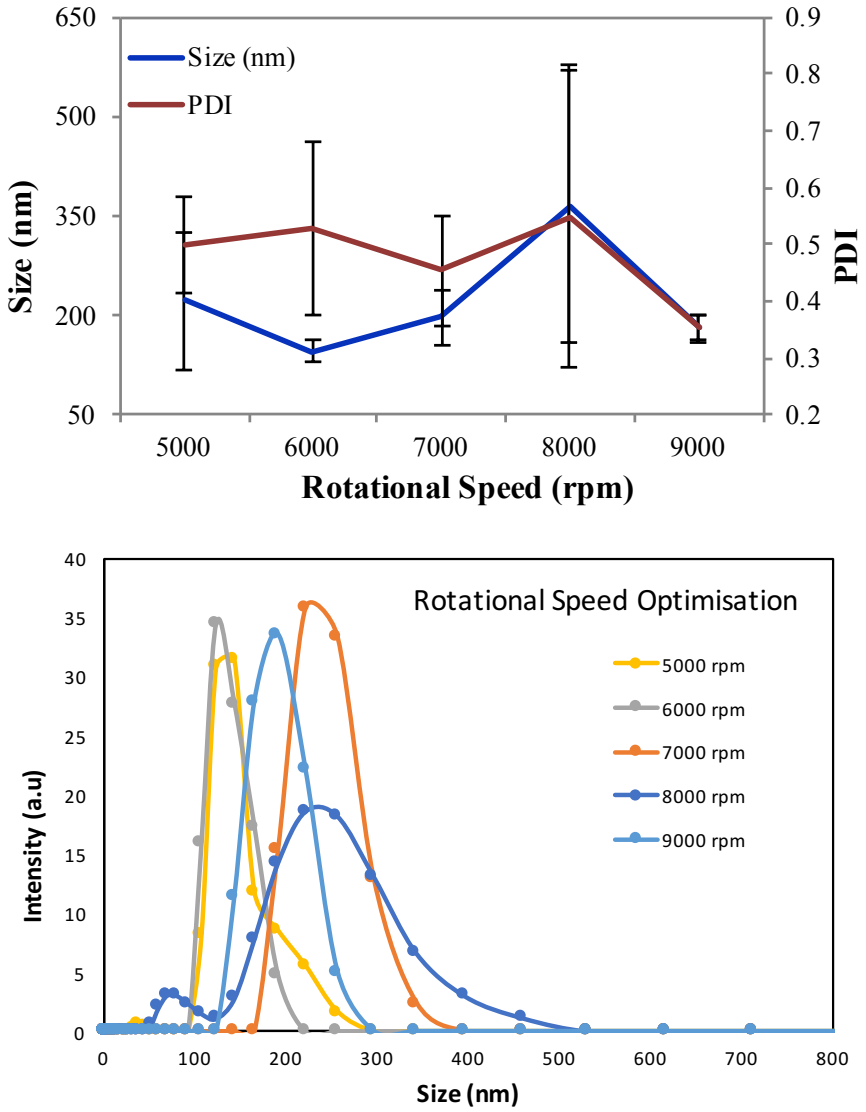

Fig S2: Phospholipid suspension at a concentration of 25 µg/mL in continuous flow at a flow rate of 0.1 mL/min, tilt angle 45° was processed at speeds 4000 rpm, 5000 rpm, 6000 rpm, 7000 rpm, 8000 rpm, 9000

rpm. All the samples were characterized at room temperature 25°C in a hydrophobic tube. All the sample measurements were repeated in triplicates and a standard error was obtained. All the samples were processed in hydrophobic coated inner surface tube with an OD 20mm.

4. Tilt angle optimization in hydrophobic tube.

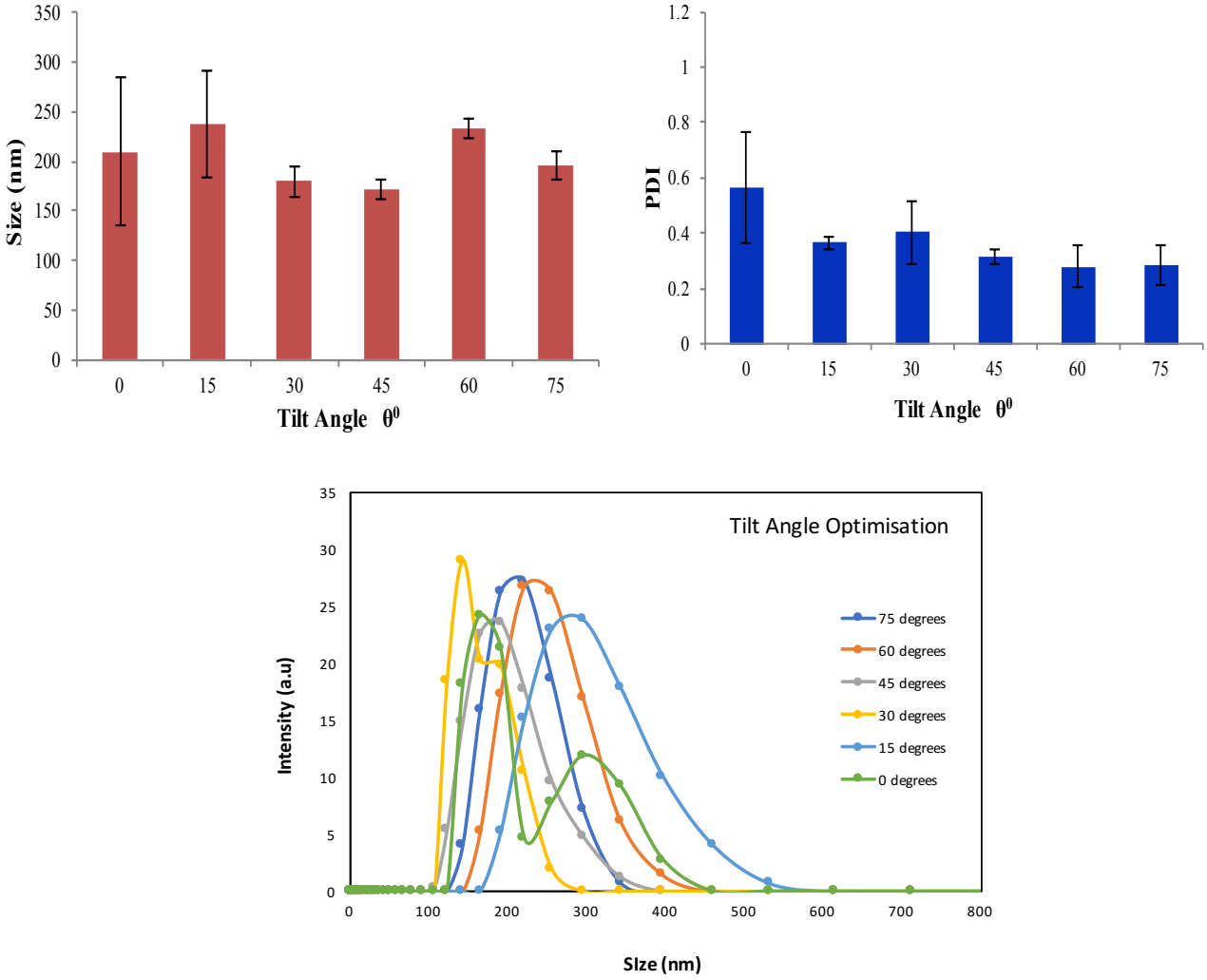

Phospholipid suspension at a concentration of 25 µg/mL in continuous flow at a flow rate of 0.1 mL/min, 9000 rpm and all the tilt angles were optimized 0°, 15°, 30°, 45°, 60°, 75° . The optimized angle was observed at 45° which is also common for a number of processing in the VFD.

Fig S3: Phospholipid suspension at a concentration of 25 µg/mL in continuous flow at a flow rate of 0.1 mL/min, 9000 rpm and all the tilt angles were optimized 0°, 15°, 30°, 45°, 60°, 75° . All the samples were

characterized at room temperature 25°C in a hydrophobic tube. All the sample measurements were repeated in triplicates and a standard error was obtained. All the samples were processed in hydrophobic coated inner surface tube with an OD 20mm.

5. Flow-rate optimization in hydrophobic tube.

Phospholipid suspension at a concentration of 25 µg/mL was processed at 9000 rpm in continuous flow at a tilt angle 45° and different flow-rates from 0.1 mL/ min, 0.3 mL/min, 0.5 mL/min, 0.7 mL/min, 1.0 mL/min were optimized. The size was observed to be around 100 nm at the lowest flow rate 0.1mL/min with low polydispersity index (PDI). Lower the flow-rate, the residence time for the samples to be processed under shear is more which impacts on the controlling the size of the self-assembly. All the measurements were conducted through DLS.

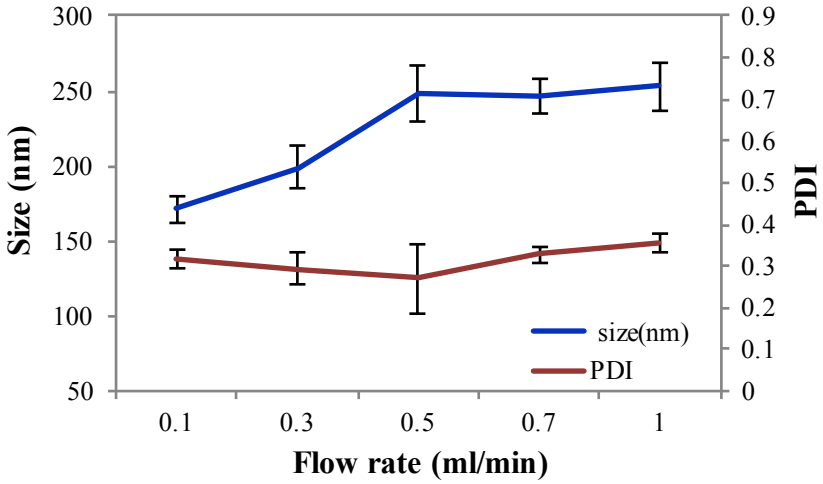

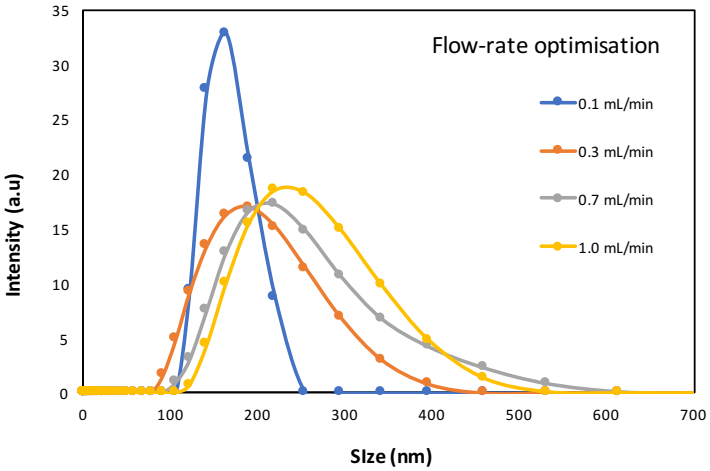

Fig S4: Phospholipid suspension at a concentration of 25 μg/mL was processed at 9000 rpm in continuous flow at a tilt angle 45° and different flow-rates from 0.1 mL/ min, 0.3 mL/min, 0.5 mL/min, 0.7 mL/min, 1.0 mL/min were optimized. All the samples were characterized at room temperature 25°C in a hydrophobic tube. All the sample measurements were repeated in triplicates and a standard error was obtained. All the samples were processed in hydrophobic coated inner surface tube with an OD 20mm.

6. Concentration optimization in hydrophobic tube.

Phospholipid suspension at a concentration of 25 μg/mL, 50 μg/mL and 1mg/mL were optimized. All the samples were processed at 9000 rpm and at a tilt angle of 45° . All the samples yielded ~ 100 nm in size. The polydispersity (PDI) was observed different at different concentrations. The PDI was lowest for 25μg/mL. Different formulations in industry requires liposomal formulation at 0.1 - 1mg/mL depending on the application. All the measurements were conducted through Dynamic Light Scattering Technique (DLS).

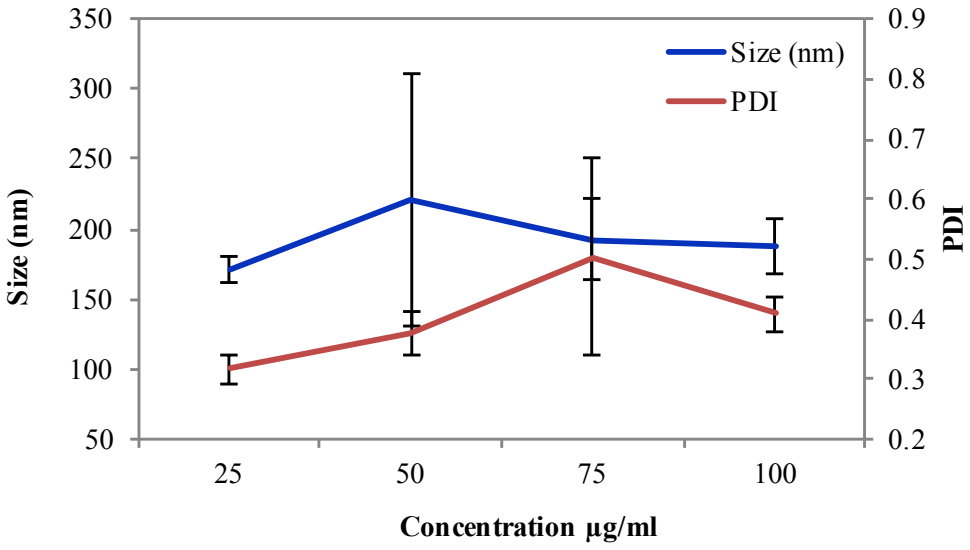

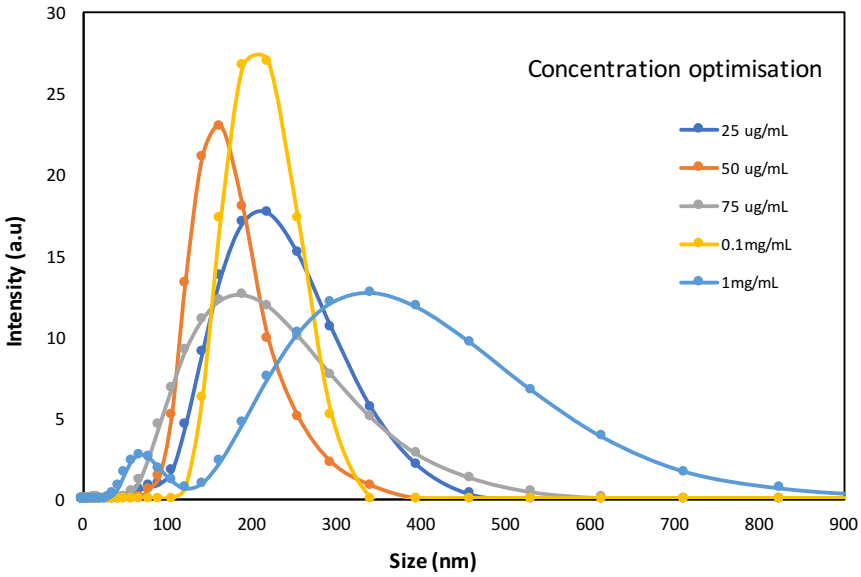

Fig S5: Phospholipid suspension at a concentration of 25 µg/mL, 50 µg/mL and 1mg/mL were optimized. All the samples were processed at 9000 rpm and at a tilt angle of 45°. All the samples were characterized at room temperature 25°C in a hydrophobic tube. All the sample measurements were repeated in triplicates and a standard error was obtained. All the samples were processed in hydrophobic coated inner surface tube with an OD 20mm.

7. Transmission Electron Microscopy (TEM) on liposomes processed in bench top vortexer.

1 mg/mL phospholipid suspension was vortexed in a vortex mixer for 15 minutes at room temperature 25°C and characterized through Transmission Electron Microscopy (TEM) for control. A similar liposome sample was observed with non-uniform sizes across the TEM grid. The liposomes processed from vortexer were highly unstable under vacuum and were squeezed in sizes as observed from the images provided.

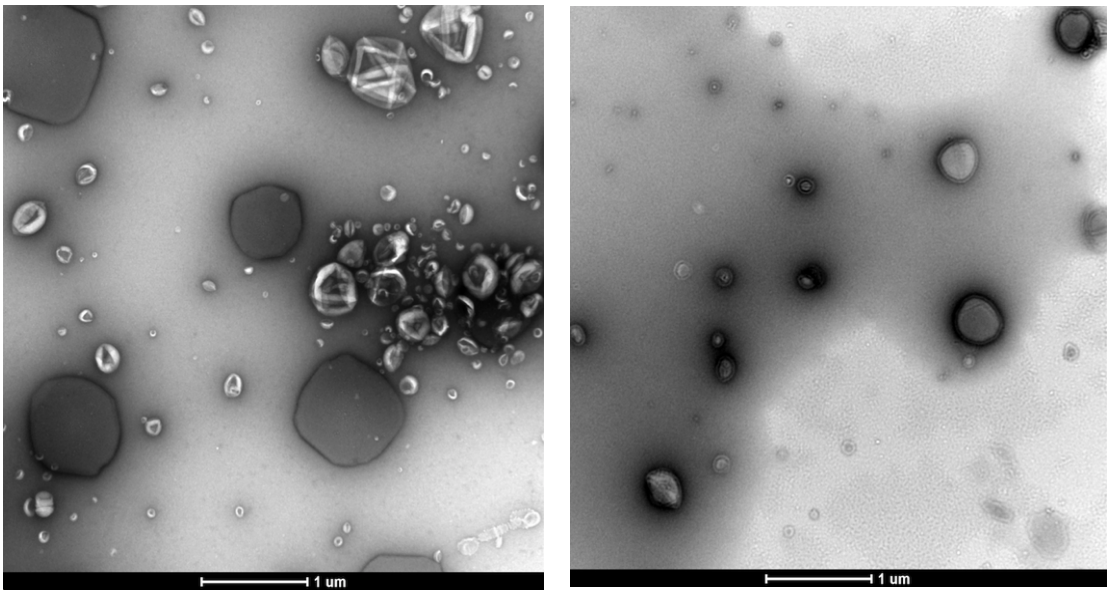

Fig S6: 1 mg/mL phospholipid suspension was vortexed in a vortex mixer for 15 minutes at room temperature 25°C. The TEM grid was plasma modified for a hydrophilic surface to obtain a better adherence of the sample. The sample was further stained by 2% uranyl acetate and 3 washes with Milli-Q water was given to obtain the final images.

8. Small Angle Neutron Scattering Analysis (SANS).

Methods:

SANS was conducted on the BILBY instrument at ANSTO (Lucas Heights, NSW, Australia). The VFD was setup in the instrument's sample staging area so scans could be made during *in-situ* VFD shearing (real-time VFD). After shearing, the sample was scanned again with static-SANS to determine if there were any lasting effects on the sample structure. The data was reduced to account for the instrument geometry and detector resolution, and for background scattering from solvent, the quartz VFD tube, and the environment. The reduced data was then set to absolute scale. The data was analyzed using the NIST macros developed for Igor Pro. The best fit for each data set is shown below. Non-resolution-smeared models were used due to the large q-resolution interfering with the quality of the fits. The choice in models as well as the significance of the fitting results can be found in the article.

POPC in D_2O, 0 rpm (Guinier-Porod Model)

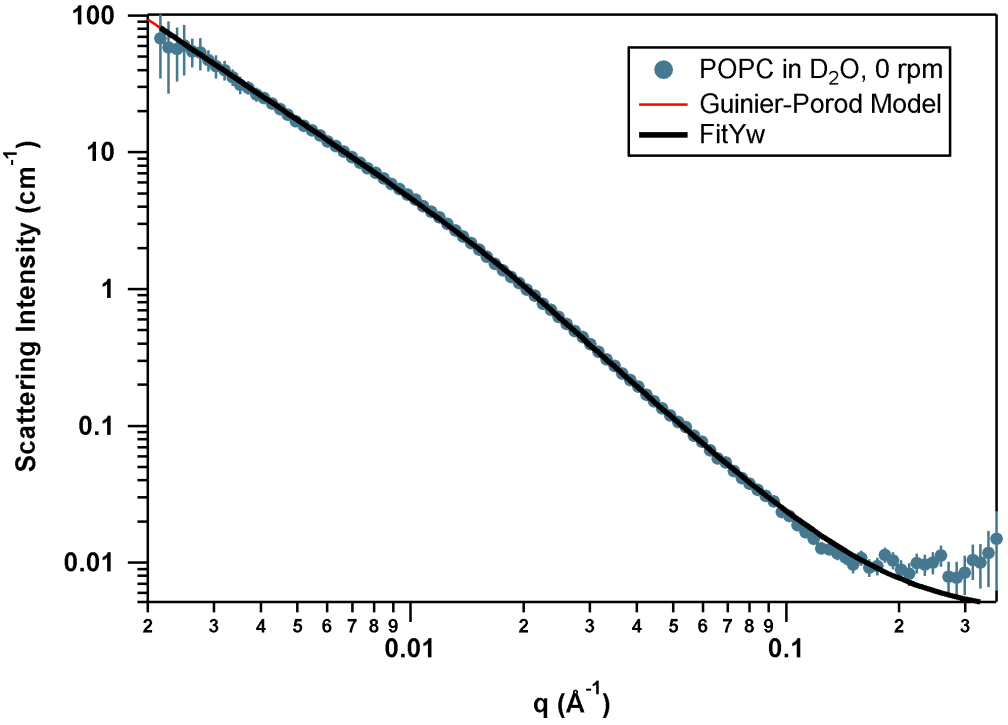

Guinier Scale	0.00110692	±	0.000162266
Dimension Variable, s	1.82569	±	0.0298152
R_g (Å)	28.8541	±	1.95334
Porod Exponent	2.47006	±	0.0131532
Bgd (cm^{-1})	0.00411191	±	0.000387157
Fitted Range	0.00216	$< q <$	0.32933
Sqrt(χ^2/N)	0.898677		

POPC in D_2O, 3800 rpm (Uniform Ellipsoid + Dilute Lamellar Model)

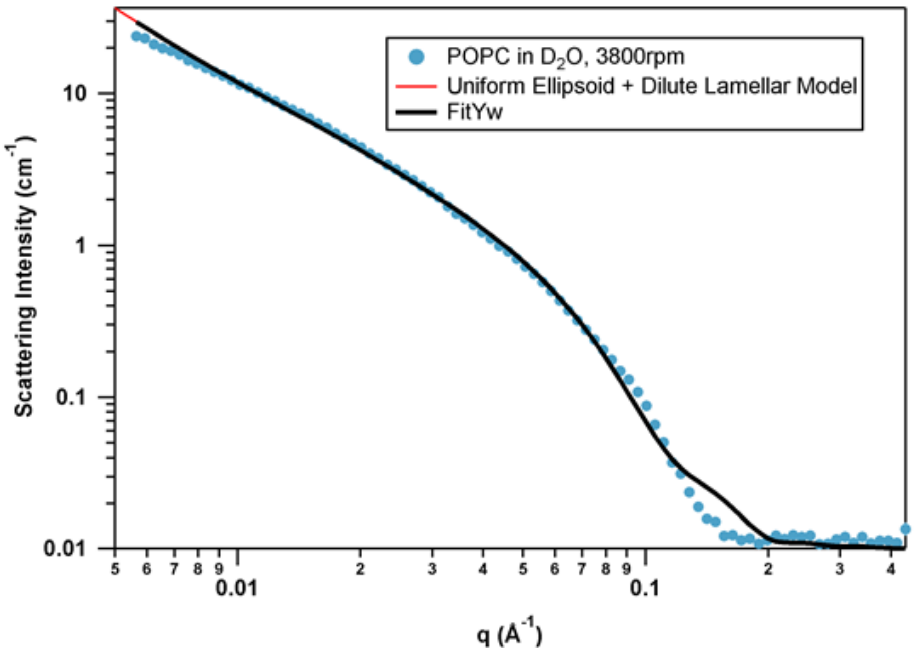

Scale	0.001797	±	8.96E-06
R_a (rotation axis) (Å)	179.805	±	3.14486
R_b (A)	35.4491	±	0.058442
SLD ellipsoid ($Å^{-2}$)	1.00E-06	±	0
SLD solvent ($Å^{-2}$)	6.30E-06	±	0
Scale	0.0017	±	1.29E-05
Bilayer Thick (delta) (Å)	26.2122	±	0.185884
polydisp of thickness	0.15	±	0
SLD bilayer (Å-2)	1.00E-06	±	0
SLD solvent (Å-2)	6.30E-06	±	0
incoh. bkg (cm-1)	0.00995	±	9.89E-05
Fitted Range	0.00565	< q <	0.43443
Sqrt(χ2/N)	10.1767		

POPC in D_2O, after 3800 rpm (Uniform Ellipsoid + Dilute Lamellar Model)

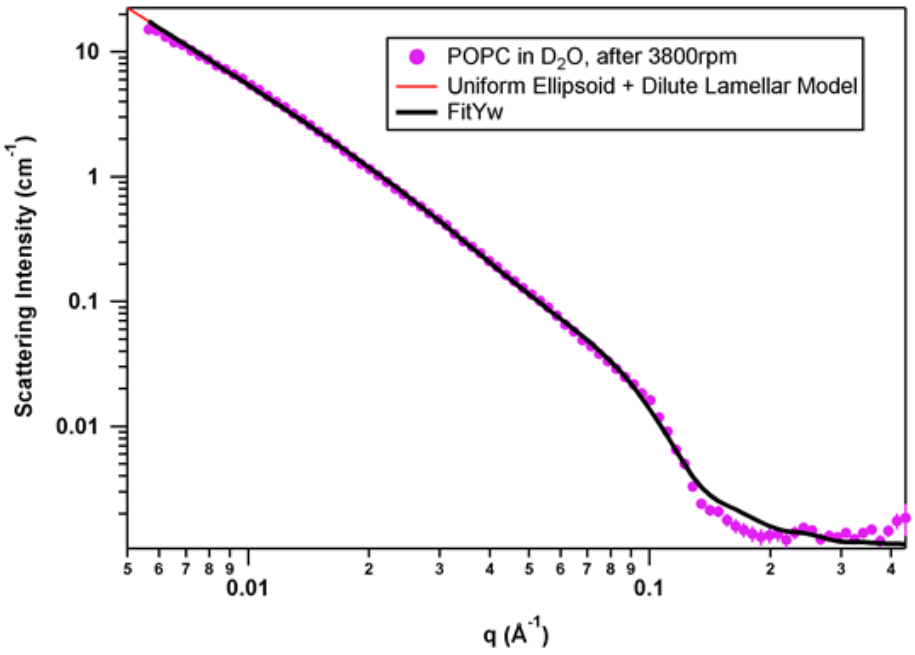

Scale	0.000345	±	3.09E-06
R_a (rotation axis) (Å)	22.2845	±	0.325682
R_b (A)	37.7535	±	0.379429
SLD ellipsoid ($Å^{-2}$)	1.00E-06	±	0
SLD solvent ($Å^{-2}$)	6.30E-06	±	0
Scale	0.000389	±	1.63E-06
Bilayer Thick (delta) (Å)	73.8369	±	0.349819
polydisp of thickness	0.35	±	0
SLD bilayer (Å-2)	1.00E-06	±	0
SLD solvent (Å-2)	6.30E-06	±	0
incoh. bkg (cm-1)	0.001116	±	3.50E-05
Fitted Range	0.00565	< q <	0.43443
Sqrt(χ2/N)	5.29794		

POPC in D_2O, 4000 rpm (Guinier-Porod + Gauss Peak Model)

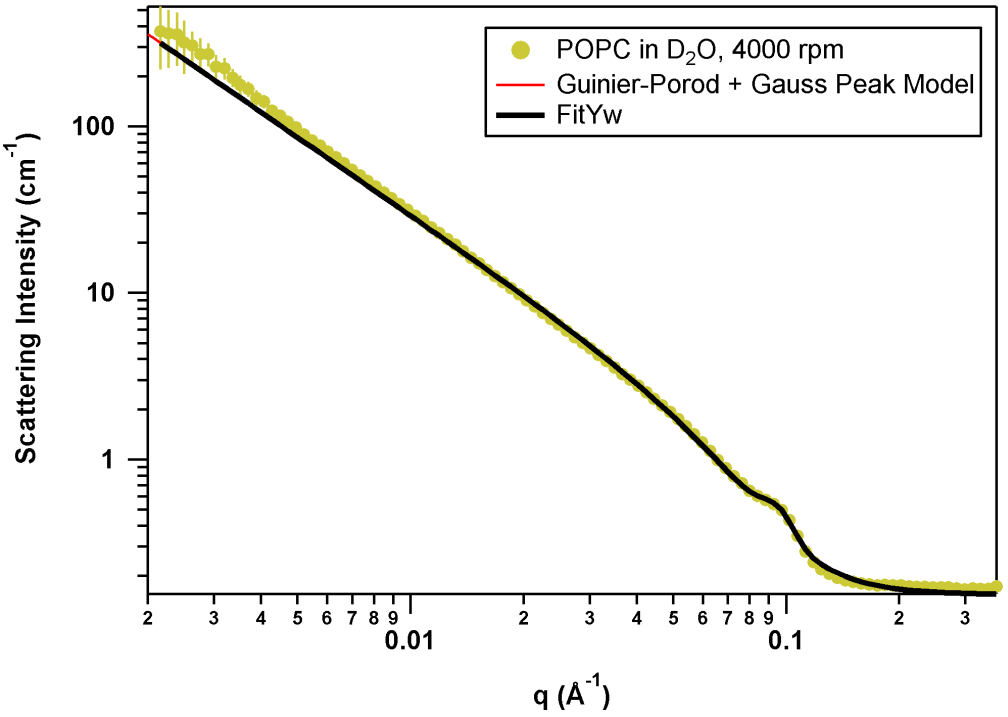

Scale Factor, I_0	0.139192	±	0.00382661
Peak position ($Å^{-1}$)	0.0939534	±	0.000283786
Std Dev ($Å^{-1}$)	0.00902009	±	0.000263683
Guinier Scale	0.02301	±	0.000695443
Dimension Variable, s	1.55297	±	0.00759616
R_g (Å)	14.7385	±	0.175632
Porod Exponent	4	±	0.0687602
Bgd (cm^{-1})	0.154588	±	0.00100337
Fitted Range	0.00216	$< q <$	0.36309
Sqrt(χ^2/N)	2.70165		

POPC in D_2O, post-4000 rpm (Guinier-Porod Model)

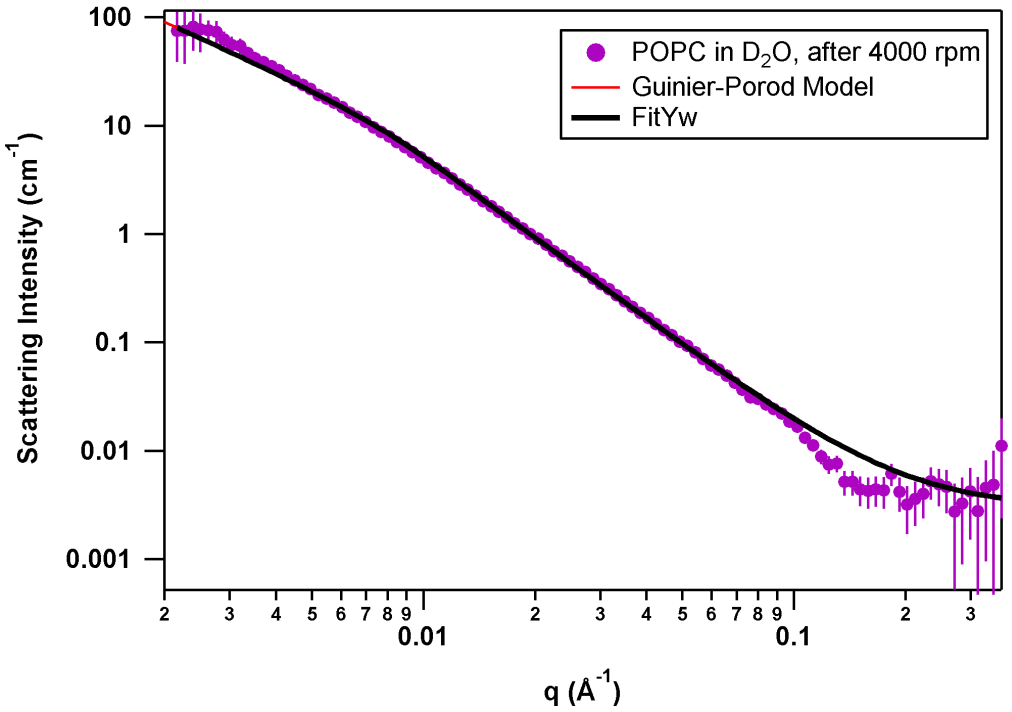

Guinier Scale	0.00748023	±	0.00066541
Dimension Variable, s	1.51611	±	0.0202529
R_g (Å)	80.6432	±	0.278793
Porod Exponent	2.49027	±	0.00647777
Bgd (cm^{-1})	0.003	±	0
Fitted Range	0.00276	$< q <$	0.3458
Sqrt(χ^2/N)	1.51097		

POPC in D_2O, 4500 rpm (Uniform Ellipsoid + Dilute Lamellar Model)

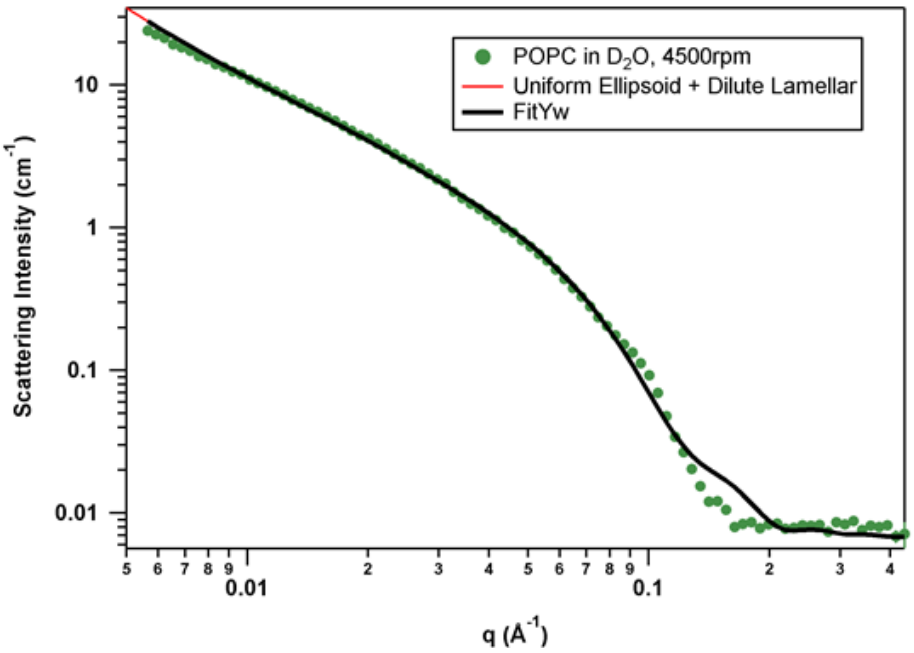

Scale	0.001936	±	9.88E-06
R_a (rotation axis) (Å)	180.268	±	3.38898
R_b (A)	33.6063	±	0.0633072
SLD ellipsoid ($Å^{-2}$)	1.00E-06	±	0
SLD solvent ($Å^{-2}$)	6.30E-06	±	0
Scale	0.001573	±	1.44E-05
Bilayer Thick (delta) (Å)	26.7727	±	0.228554
polydisp of thickness	0.15	±	0
SLD bilayer ($Å^{-2}$)	1.00E-06	±	0
SLD solvent ($Å^{-2}$)	6.30E-06	±	0
incoh. bkg (cm^{-1})	0.006663	±	0.000107749
Fitted Range	0.00565	< q <	0.43443
Sqrt(χ^2/N)	8.13027		

POPC in D_2O, after 4500 rpm (Dilute Lamellar Model)

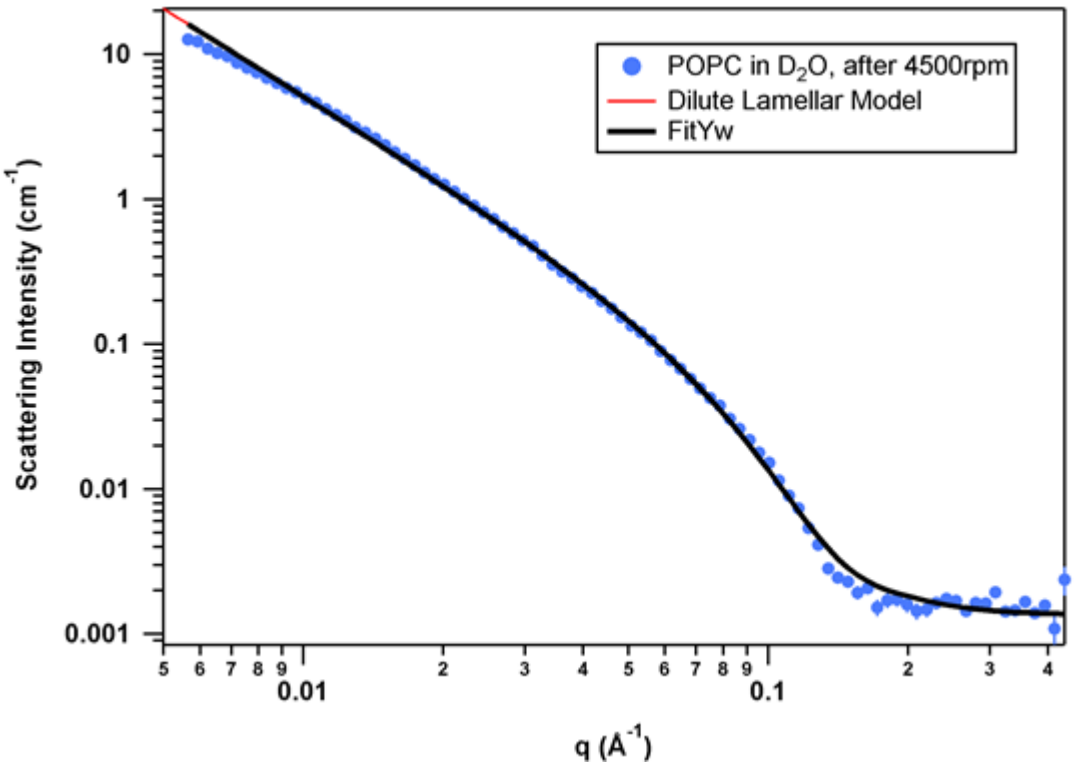

Scale	0.0007794	±	3.38E-06
Bilayer Thick (delta) (Å)	34.1438	±	0.416763
polydisp of thickness	0.324893	±	0.0142523
SLD bilayer ($Å^{-2}$)	1.00E-06	±	0
SLD solvent ($Å^{-2}$)	6.30E-06	±	0
incoh. bkg (cm^{-1})	0.0013506	±	3.67E-05
Fitted Range	0.00565	< q <	0.43443
Sqrt(χ^2/N)	9.1285		

POPC in D_2O, 5000 rpm (Guinier-Porod Model)

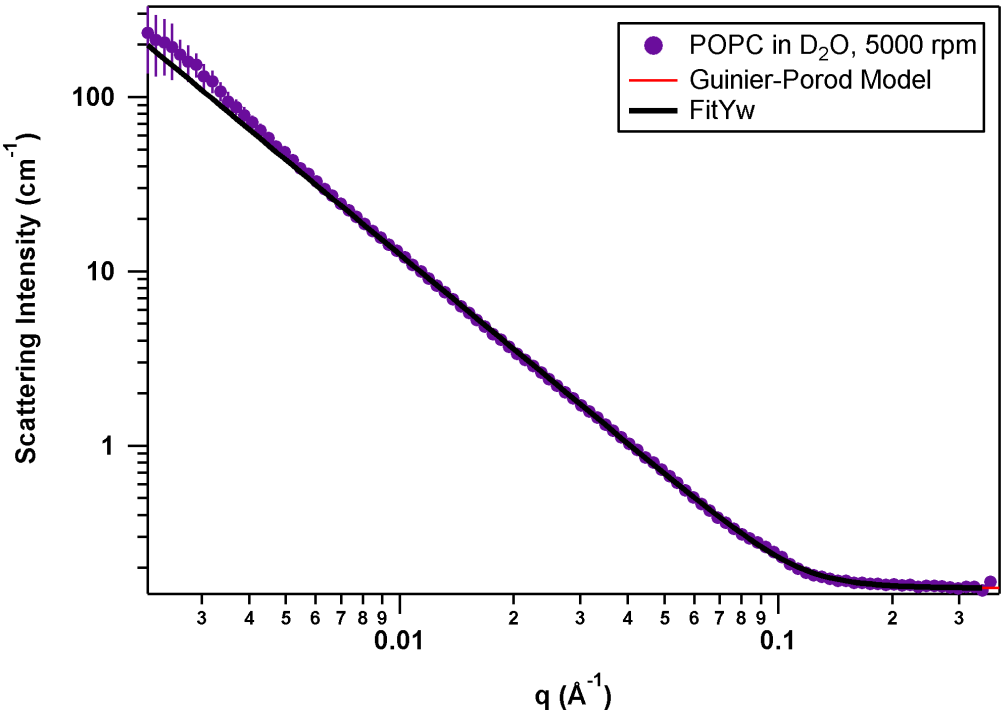

Guinier Scale	0.00305	±	7.34E-05
Dimension Variable, s	1.80577	±	0.00622
R_g (Å)	10.5009	±	0.14143
Porod Exponent	4	±	0.25058
Bgd (cm^{-1})	0.15224	±	0.00111
Fitted Range	0.00216	< q <	0.3458
Sqrt(χ^2/N)	1.27927		

POPC in D_2O, post-5000 rpm (Guinier-Porod + Gauss Peak Model)

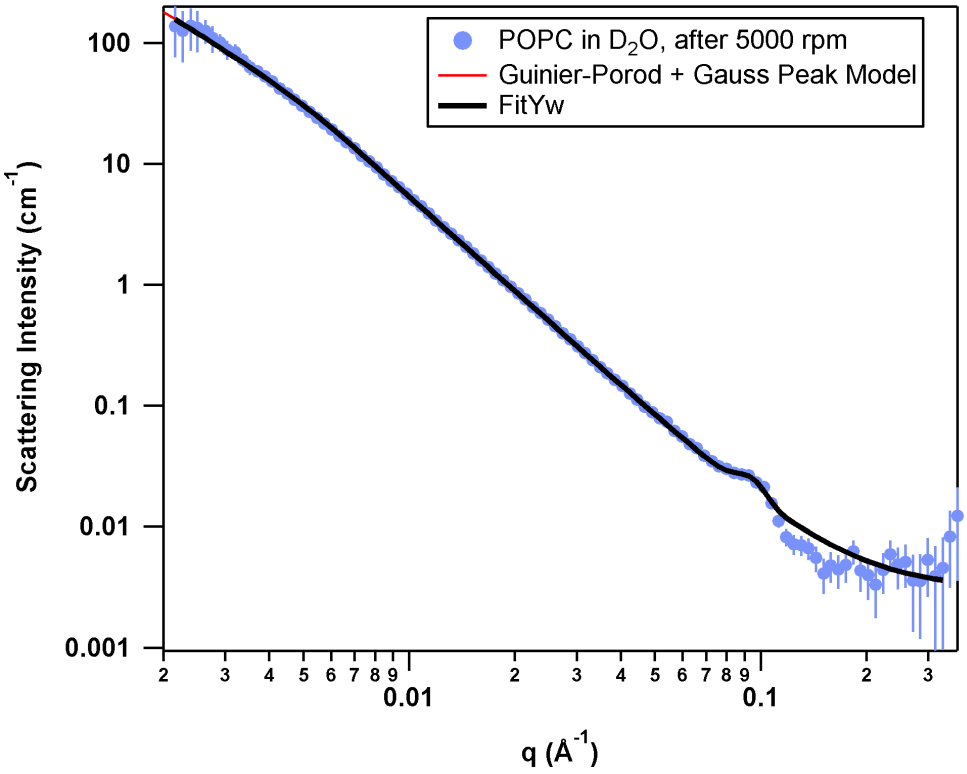

Scale Factor, I_0	0.00672427	±	0.00105872
Peak position ($Å^{-1}$)	0.0932791	±	0.00134198
Std Dev ($Å^{-1}$)	0.00861001	±	0.00133965
Guinier Scale	0.0050925	±	0.000934891
Dimension Variable, s	1.69039	±	0.0398115
R_g (Å)	114.747	±	0.429865
Porod Exponent	2.60294	±	0.00614766
Bgd (cm^{-1})	0.003	±	0
Fitted Range	0.00216	$< q <$	0.32933
Sqrt(χ^2/N)	0.774034		

POPC in D_2O, 6000 rpm (Guinier-Porod Model)

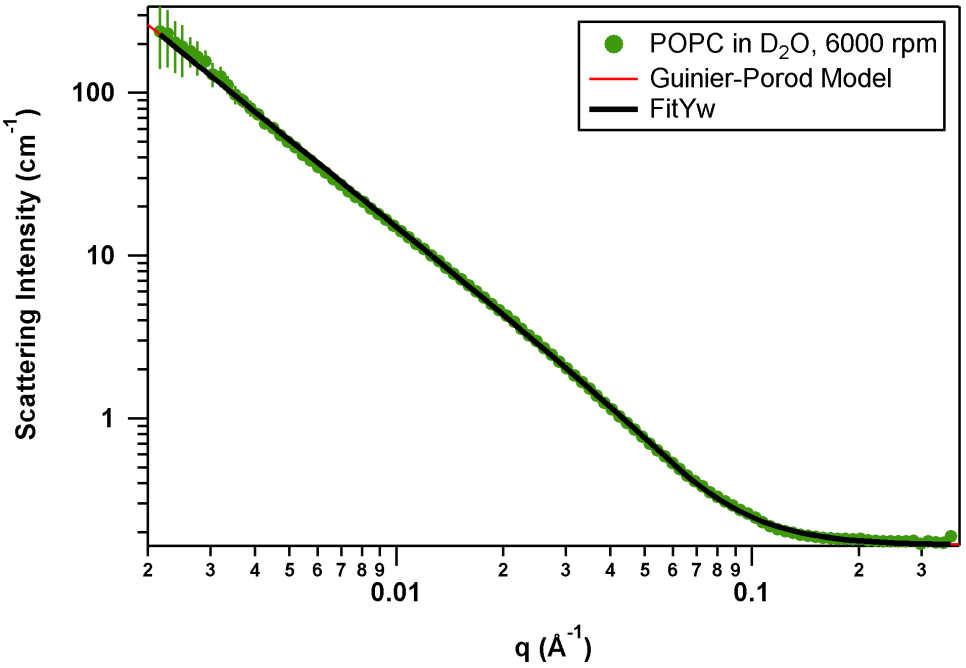

Guinier Scale	0.00428341	±	0.00015001
Dimension Variable, s	1.77356	±	0.00843036
R_g (Å)	13.7566	±	0.226353
Porod Exponent	2.90742	±	0.0328794
Bgd (cm^{-1})	0.165793	±	0.000871873
Fitted Range	0.00216	$< q <$	0.3458
Sqrt(χ^2/N)	1.39376		

POPC in D_2O, post-6000 rpm (Guinier-Porod + Gauss Peak Model)

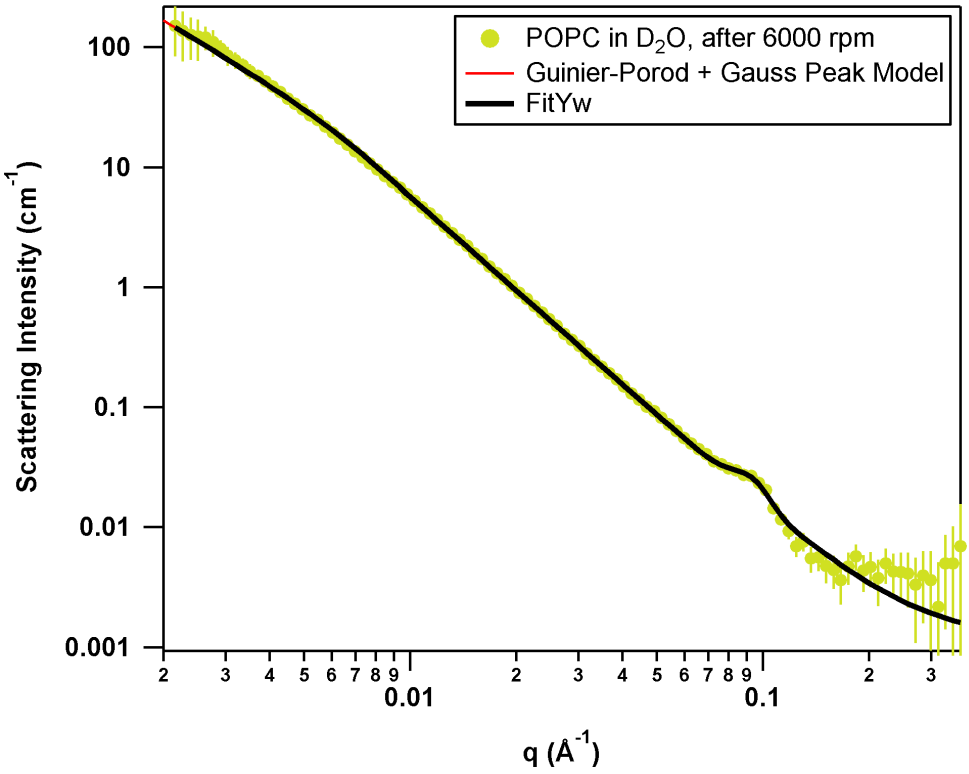

Scale Factor, I_0	0.00797113	±	0.000928219
Peak position ($Å^{-1}$)	0.0908765	±	0.0014001
Std Dev ($Å^{-1}$)	0.0106605	±	0.00151128
Guinier Scale	0.00467428	±	0.00066991
Dimension Variable, s	1.69206	±	0.0309262
R_g (Å)	99.1467	±	0.365561
Porod Exponent	2.60665	±	0.00749214
Bgd (cm^{-1})	0.00111015	±	0.000361253
Fitted Range	0.00216	$< q <$	0.36309
Sqrt(χ^2/N)	0.663647		

POPC in D_2O, 7000 rpm (Guinier-Porod Model)

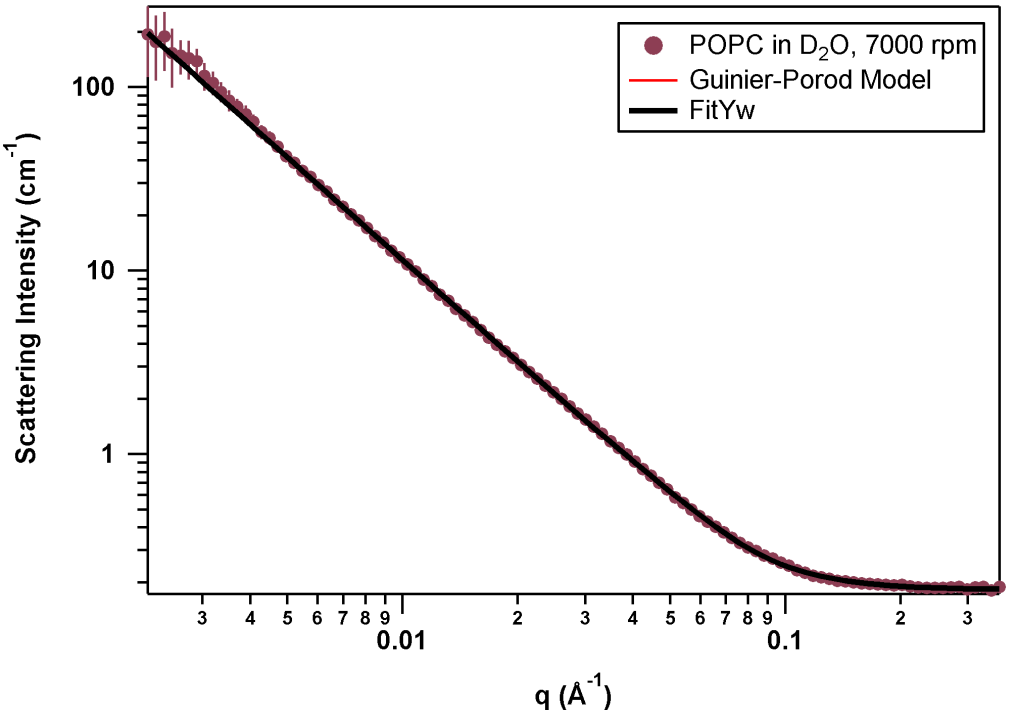

Guinier Scale	0.00218	±	6.8E-05
Dimension Variable, s	1.85945	±	0.00773
R_g (Å)	10.7583	±	0.19991
Porod Exponent	2.98729	±	0.0743
Bgd (cm^{-1})	0.18248	±	0.00108
Fitted Range	0.00216	< q <	0.36309
Sqrt(χ^2/N)	0.883602		

POPC in D_2O, post-7000 rpm (Guinier-Porod + Gauss Peak Model)

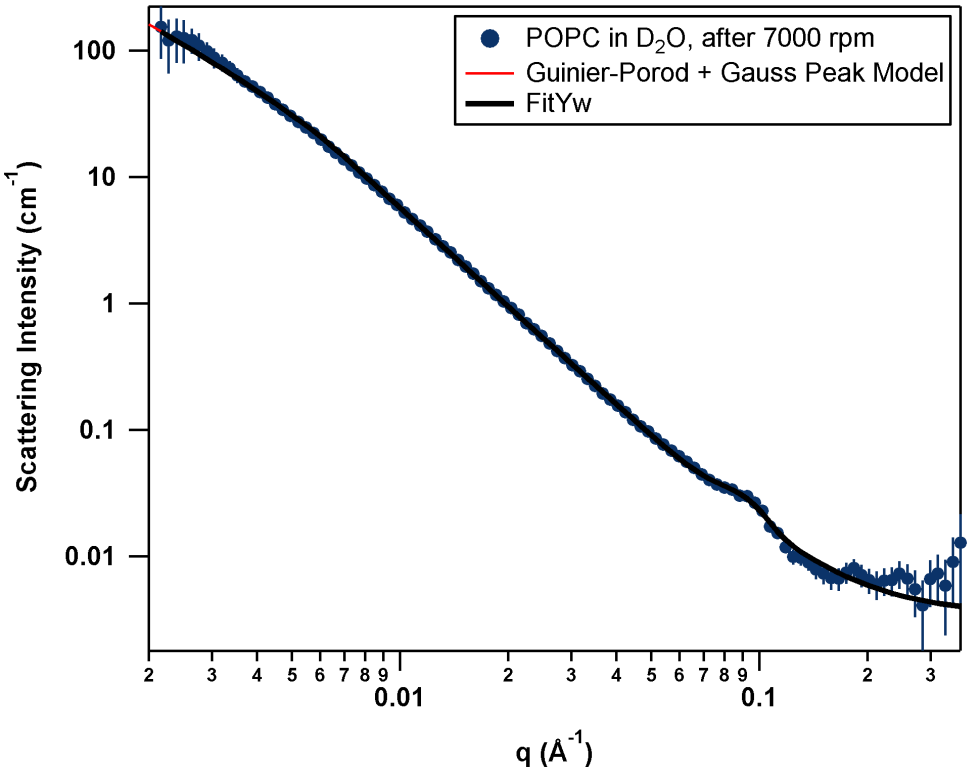

Scale Factor, I_0	0.00768447	±	0.000824106
Peak position ($Å^{-1}$)	0.088101	±	0.00164059
Std Dev ($Å^{-1}$)	0.0136022	±	0.001821
Guinier Scale	0.00935576	±	0.00153752
Dimension Variable, s	1.57566	±	0.0351863
R_g (Å)	117.936	±	0.384538
Porod Exponent	2.5957	±	0.00744541
Bgd (cm^{-1})	0.00350533	±	0.000363918
Fitted Range	0.00216	$< q <$	0.36309
Sqrt(χ^2/N)	0.708935		

POPC in D_2O, 8000 rpm (Guinier-Porod Model)

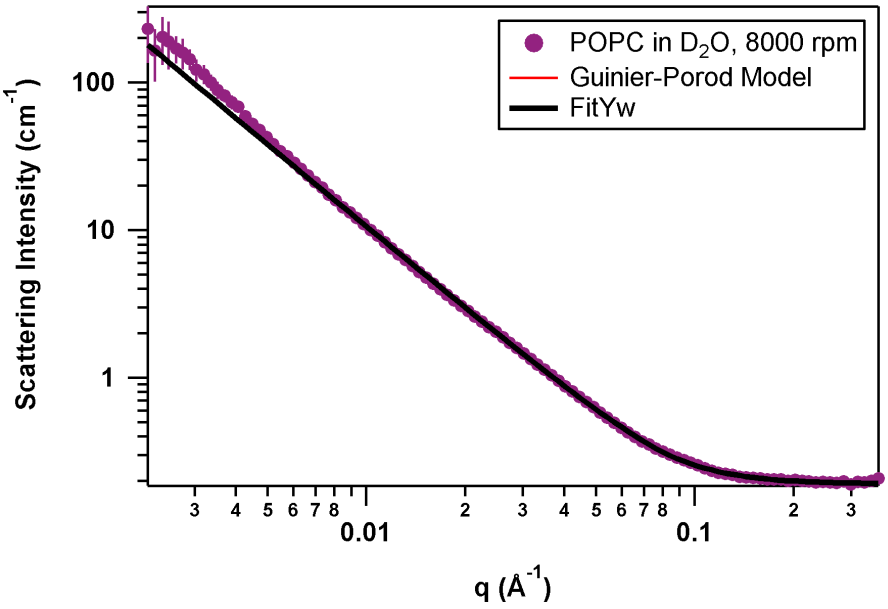

Guinier Scale	0.00208	±	6.99E-05
Dimension Variable, s	1.85289	±	0.00827
R_g (Å)	10.466	±	0.22502
Porod Exponent	2.83277	±	0.06875
Bgd (cm^{-1})	0.19065	±	0.00116
Fitted Range	0.00216	< q <	0.36309
Sqrt(χ^2/N)	1.127		

POPC in D_2O, post-8000 rpm (Guinier-Porod + Gauss Peak Model)

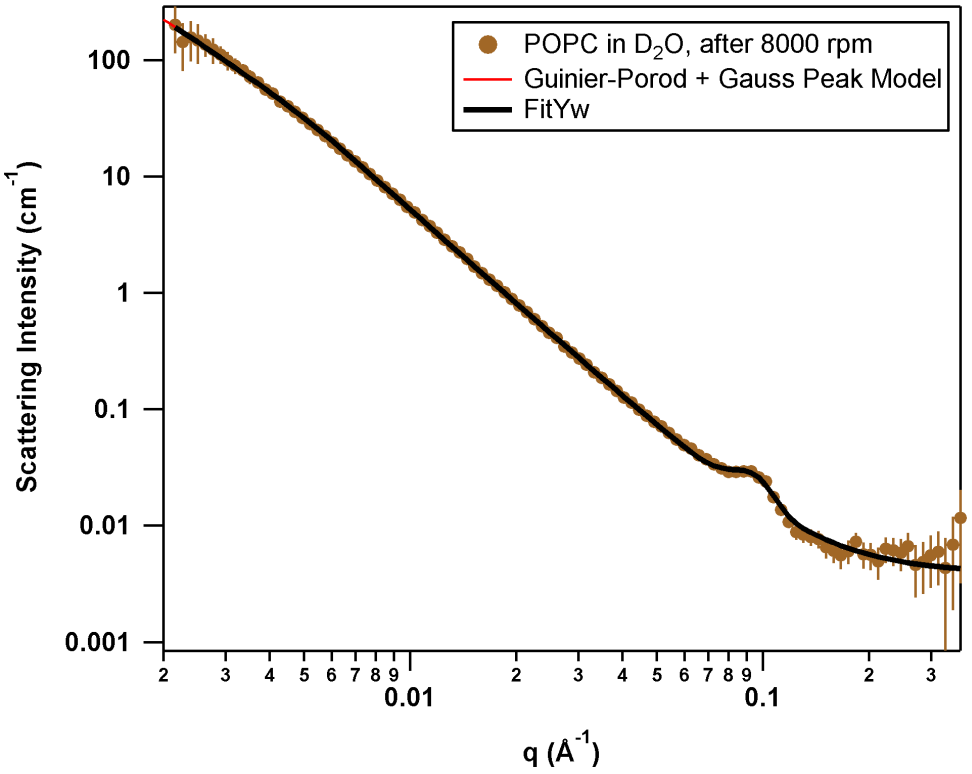

Scale Factor, I_0	0.0110771	±	0.000859821
Peak position ($Å^{-1}$)	0.0921981	±	0.00105007
Std Dev ($Å^{-1}$)	0.012151	±	0.00114793
Guinier Scale	0.00155857	±	0.000311834
Dimension Variable, s	1.91627	±	0.0437406
R_g (Å)	99.2896	±	0.46333
Porod Exponent	2.67582	±	0.00760261
Bgd (cm^{-1})	0.00394246	±	0.000355445
Fitted Range	0.00216	$< q <$	0.36309
Sqrt(χ^2/N)	0.571722		

POPC in D_2O, 9000 rpm (Guinier-Porod Model)

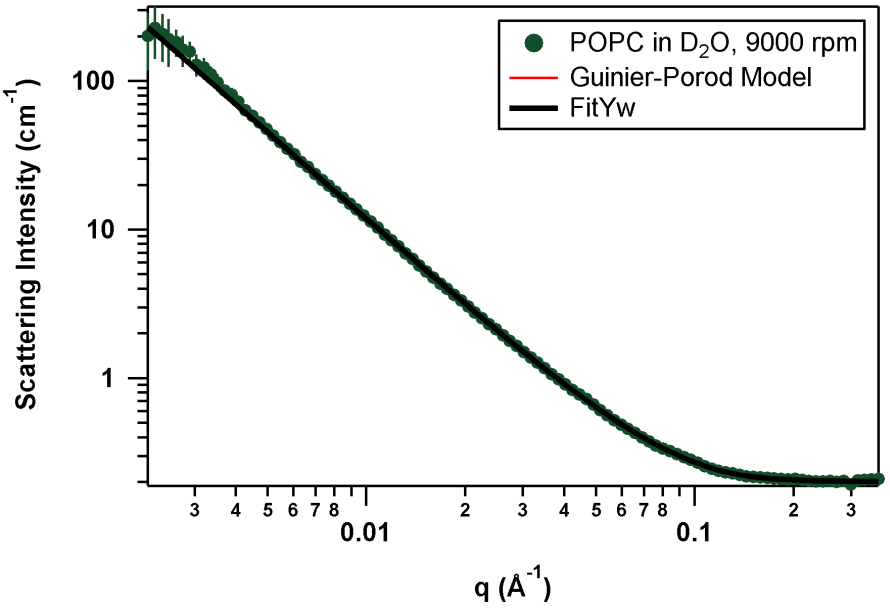

Guinier Scale	0.00153	±	3.96E-05
Dimension Variable, s	1.94189	±	0.00656
R_g (Å)	8.23756	±	0.21404
Porod Exponent	3.59712	±	0.39886
Bgd (cm^{-1})	0.20111	±	0.00175
Fitted Range	0.00216	< q <	0.36309
Sqrt(χ^2/N)	0.696727		

POPC in D_2O, post-9000 rpm (Guinier-Porod + Gauss Peak Model)

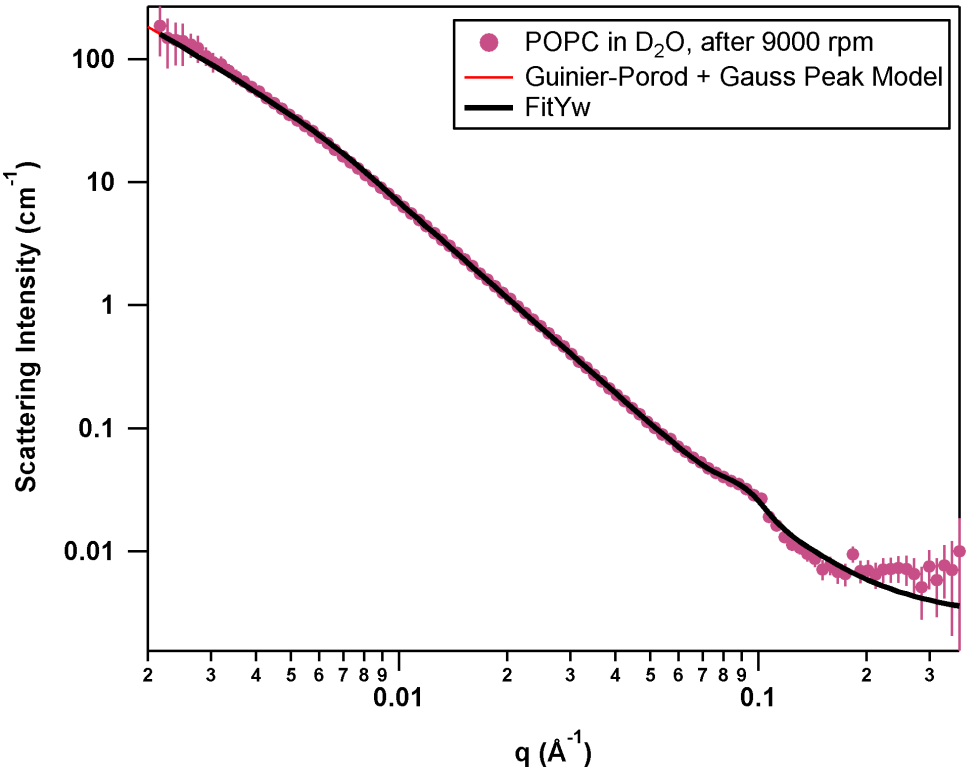

Scale Factor, I_0	0.00766825	±	0.000882325
Peak position ($Å^{-1}$)	0.0889783	±	0.00155343
Std Dev ($Å^{-1}$)	0.0121202	±	0.00169998
Guinier Scale	0.00710213	±	0.000954146
Dimension Variable, s	1.63865	±	0.0283447
R_g (Å)	98.6048	±	0.324708
Porod Exponent	2.58657	±	0.00712257
Bgd (cm^{-1})	0.00296336	±	0.000363461
Fitted Range	0.00216	$< q <$	0.36309
Sqrt(χ^2/N)	0.758237		

References.

1. Britton, J., & Raston, C. L. , *Multi-step continuous-flow synthesis.* Chemical Society Reviews, 2017. **46**(5): p. 1250.